First Principles study of novel properties of pristine and carbon supported GaX (X=P, As, Sb)

Demmilash Kassa

A Thesis submitted to
The Department of Physics

Presented in Partial fulfilment of the Requirements for the Degree of Master of Science (Physics)

Addis Ababa University
Addis Ababa, Ethiopia
November 2023

Addis Ababa University
College of Natural Sciences
School of Graduate Studies

This is to certify that the thesis prepared by Demmilash Kassa entitled: *First Principles study of novel properties of pristine and carbon supported GaX (X=P, As, Sb)* and submitted in partial fulfillment of the requirements for the Degree of Master of Science complies with the regulations of the University and meets the accepted standards with respect to originality and quality.

Signed by the Examining Committee:

Examiners

1. Dr. Lemi Demeyu Signature .... Date ....

2. Dr. Yitageu Elfagd Signature .... Date ....

Advisor(s)

1. Dr. Kenate Nemera Signature .... Date ....

Chair of Department or Graduate Program Coordinator

Date: **10/11/23**

Author: **Demmilash Kassa**

Title: **First Principles study of novel properties of pristine and carbon supported GaX (X=P, As, Sb)**

Department: **Physics**

Degree: **MSc** Convocation: **November** Year: **2023**

Permission is here with granted to Addis Ababa University to circulate and to have copied for non-commercial purposes, at its discretion, the above title upon the request of individuals or institutions.

Signature of Author

THE AUTHOR RESERVES OTHER PUBLICATION RIGHTS, AND NEITHER THE THESIS NOR EXTENSIVE EXTRACTS FROM IT MAY BE PRINTED OR OTHERWISE REPRODUCED WITHOUT THE AUTHORS WRITTEN PERMISSION.

THE AUTHOR ATTESTS THAT PERMISSION HAS BEEN OBTAINED FOR THE USE OF ANY COPYRIGHTED MATERIAL APPEARING IN THIS THESIS (OTHER THAN BRIEF EXCERPTS REQUIRING ONLY PROPER ACKNOWLEDGEMENT IN SCHOLARLY WRITING) AND THAT ALL SUCH USE IS CLEARLY ACKNOWLEDGED.

Abstract

Utilizing the most recent Density Functional Theory(DFT), the electronic structure,optical properties, and new characteristics of pristine and carbon-supported GaX (X=P, As, Sb) in cubic zinc-blende (ZB) phase are investigated.
For the purpose of predicting the ZB phase , the lattice parameters, bulk modulus,cohesive energy , formation energy as well as energy band nature and band gap values, and optical properties were analyzed. Where accessible, the experimental data are quite compatible with our findings and results. As compared to the experimental data, our estimated values for the equilibrium lattice parameter, bulk modulus, energy band gap, cohesive energy, and formation energy. GaP, GaAs, and GaSb results were provided as 5.54 Å, 5.65 Å, 6.21 Å, and 77.3 GPa, 52.4 GPa, and 46.0 GPa respectively for lattice parameter values and bulk modules, which are in good agreement with the experimental values. The computed cohesive energy and formation energy 1.43 eV, 3.74 eV,3.24 eV & -0.57 eV, 0,81 eV, -0.56 eV respectively, which are in a good agreement with the experimental values. Projector augmented-wave pseudo-potential (PAW) was used in the GGA,PBE, and DFT+U approximations to treat the interaction between the core and valence electrons for the minimal energy emerges. DOS and PDOS were analyzed in the electronic characteristics of the graphene/GaX (X=P, As, Sb) heterostructure from better charge. The findings indicate that there is charge transfer between graphene and GaX (X=P, As, Sb) and that the combination/junction is a conductor with no band gap. The refractive index, optical conductivity, and refelectivity of the optical characteristics studied are in good agreement with the experimental values. The most favorable adsorptions have adsorption energies in the range [-58.47,-17.07, 8.15]eV for a carbon adsorbate at 1 ML adsorbate coverage. With the adsorption of graphene, these values are in the range of [22.16,34.76, 48.63]eV. The fact that carbon has comparatively lower adsorption energies than graphene may mean that the two ions are more mobile in the electrolyte.
Additionally, with higher fuel supplies, GaSb is a more favorable and reactive surface with the adsorbates as a result, it more accurately depicts the usual surface of the GaAs alloy. Each carbon atom appears to emit roughly 0.261e of charge, which contributes power to the system.
Finally, since graphene's Dirac point is unaltered despite its adsorption on GaX, its interaction with GaX has no bearing on the significance of its higher conductivity excited electrons in hybrid systems are largely accumulated on graphene with energies between 0 and 3eV (versus Fermi energy). The calculations provide a theoretical defense for the efficient performance of graphene/GaX hybrid materials as photocatalysts and solar cells.

Acknowledgments

First of all my great sincere appreciation and praise worthy goes to our Almight **God** for giving me the strength and for hope that keeps me believing that would be possible and more interested throughout the course of my thesis work. I would like to express my sincerest appreciation to my advisor and instructor **Dr.Kenate Nemera**, whose thoughtful consideration and guidance has been invaluable for providing me the opportunity to work with him. Without his guidance, for his constructive comments,and suggestions from the beginning to end,in this thesis work would have not been become visible support and inspiration during the most critical period of my thesis and I would not have been able to accomplish this my thesis.

His continuous encouragement and critical comments were decisive to come out with the current shape of the paper thesis approach towards thesis has always inspired me and motivated me to learn more. His discourses on various aspect of computational material science will always help me think critically.

I would also like to thank him for supporting me while discussing in the class some part of the course that is related to my topic and the concept of DFT. I wish to him success, peace and grace throughout his life, forever.

I would like to thank Ministry of Education for providing me with the financial support that I required for my study and to undertake the MSc research work.

Finally, I would like to extend my compliments to my wife wezaro **Elfu Deresa** and my families for their moral, financial and material support. I also express my sincere thanks to **physics department of Addis Ababa University** for facilitating conditions for specialization in **Simulation and Modeling novel materials** master in physics and I acknowledge **MoE** for sponsoring me to work for my master(MSc) degree.

Abbreviations and Acronyms

GaP	Gallium Phosphide
GaAs	Gallium Arsenide
GaSb	Gallium Antimonide
eV	electron Volt
PAW	Projector Agumented Wave
PAPW	Projector Agumented Plane Wave
ZB	Zinc Blende
RS	Rock Salt
LED	Light Emitting Doide
DFT	Density Function Theory
DFPT	Density Functional Perturbation Theory
LDA	Local Density Approximation
GGA	Generalized Gradient Approximation
PBE	Perdew-Burke, and Ernzerhof
HK	Hohenberg Kohn
KS	Kohn-Sham
PW-PP	Plane-Wave Pseudo-Potentials
BZ	Brillion Zone
Gpaw	General
PWscf	Plane wave self-consistent field
XC	Exchange-Correlation
EOS	Equation Of State
USPP	Ultra-Soft Pseudo-Potentials
NCPP	Norm-Conserving Pseudo-Potentials
XCrySDen	X-Window Crystalline Structures and Densities
PDOS	Projected Density of States
DOS	Density of States
vdw	van der waals
ASE	Atomic Simulation Enviroment
V_{ext}	External Potential
fcc	face-centered-cubic
BSE	Bethe Sternheimer Equation
rpa	random phase approximation
IC	Integrated Circuit
IR	Infarerd
E_f	Formation Energy
E_{coh}	Cohesive Energy
B	Bulk modulus
E	Energy

E_g	Energy gap
Pbc	Periodic boundary condition
R	Reflectivity or Reflectance
n	Refractive index
α_{abs}	absorption coefficient
ε	Dielectric constant
T	Transmittance
κ_e	extinction coefficient
L	Energy Loss Spectrem
χ_E	Energy Loss Spectrem
CBE	Conduction Band Minimum
VBE	Valance Band Minimum
PBEO	Conduction Band Minimum
ACF	Atomic Charge File
AVF	Atomic Volume File
BCF	Bader Charge File

Contents

Abstract ii

1 Introduction 1

1.1 Statement of the Problem . . . 2

1.2 Significance of the study . . . 3

1.3 Objectives . . . 4

1.3.1 General Objectives . . . 4

1.3.2 Specific Objectives . . . 4

1.4 Outline of the Thesis . . . 4

2 Literature Review 5

2.1 Density Functional Theory . . . 5

2.1.1 Introduction . . . 5

2.1.2 Hamiltonian of Electronic system . . . 6

2.1.3 The Hartree Method . . . 7

2.1.4 Hartree-Fock Method . . . 8

2.1.5 Born-Oppenheimer Approximation . . . 8

2.1.6 The Hohenberg-Kohn Theorem . . . 10

2.1.7 The Kohn-Sham Equations . . . 10

2.1.8 Variational Principle . . . 12

2.1.9 The Exchange-Correlation Functional (E_{xc}) . . . 12

2.1.10 The Bloch Theorem . . . 16

2.2 Crytal Structure of GaX (X=P, As, Sb) . . . 16

2.2.1 The Electronic Properties of GaX (X=P, As, Sb) . . . 19

2.2.2 Geometry Optimization . . . 21

2.3 Optical Propeties of GaX (X=P, As, Sb) . . . 21

2.4 Structural, Electronic, and Optical properties of Graphene . . . 25

2.4.1 Structural properties of Graphene . . . 25

2.4.2 Electronic properties of graphene . . . 25

2.5 Absroption Energy of GaX (X=P, As, Sb) on graphene . . . 26

2.5.1 Spin polarization . . . 27

3 Methodology 28

3.1 Implementation of Density functional theory(DFT) . . . 28

3.1.1 Hubbard U scheme (DFT+U) . . . 28

3.1.2 GPAW code . . . 29

3.1.3 Technical Detail Convergence test . . . 30

3.1.4 Spin polarization . . . 34

4 Results and Discussion **35**
4.1 Result of DFT . . . 35
4.1.1 Bulk Properties of GaX . . . 35
4.1.2 Electronic Properties of GaX . . . 39
4.1.3 Optical Properties of zinc-blende (ZB) GaX (X=P, As, Sb) . 42
4.2 Structural and Electronic properties of graphene/GaX(X=P, As, Sb) heterostructure . . . 47
4.2.1 Structural properties of graphene/GaX (X=P, As, Sb)heterojunction 47

5 Conclusion and Recommendations **60**
5.1 Conclusion . . . 60
5.2 Recommendation and future work . . . 61

Bibliography **62**

List of Figures

2.1 Cubic zinc-blende structures of GaX . . . 18
2.2 Crystal structure of GaX . . . 18
2.3 Crystal structure of GaX . . . 19
2.4 structural properties of graphene . . . 26

3.1 Truncating the plane wave expansion. . . . 30
3.2 Approximations of Pseudopotentials . . . 33

4.1 Total energy versus Lattice constant of GaX . . . 37
4.2 Convergence test of the total energy versus to k-point sampling of GaX . . . 38
4.3 Convergence test of the total energy versus to ecut sampling of GaX 39
4.4 Band structure of zinc-blende GaX (X = P, As and Sb) from GGA calculation at 0 K . . . 40
4.5 Density of States for GaP, GaAs and GaSb . . . 41
4.6 Partial Density of States for GaP, GaAs and GaSb . . . 41
4.7 Calculated BSE data for complex dielectric constant for ZB of GaX 42
4.8 Calculated RPA data for real and imaginary parts of dielectric constant for ZB of GaX . . . 43
4.9 Refractive Index for ZB structures of GaX . . . 45
4.10 Absorption Coefficient for ZB structures of GaX . . . 45
4.11 Reflectance for ZB structures of GaX . . . 47
4.12 Graphene/GaX heterojunction structure . . . 48
4.13 Cohesive Energies versus equilibrium distance(d) GaP,GaAs and GaSb materials systems of Heterostructure . . . 50
4.14 Formation Energies versus equilibrium distance(d) GaP,GaAs and GaSb materials systems of Heterostructure . . . 51
4.15 Energy per atom versus equilibrium distance(d) GaP,GaAs and GaSb materials systems of Heterostructure . . . 52
4.16 Density of state heterostructure for GaX (X = P, As and Sb) . . . 53
4.17 Bader electronic charge density Zinc-Blende(ZB) of GaX (X = P, As and Sb) . . . 59

List of Tables

4.1 Computed the lattice constant $a(\ \AA)$, the bulk modulus $B(GPa)$, formation energy $E_f(eV/atom)$, and the cohesive energies $E_{coh}(eV/atom)$ of selected GaX or GaP,GaAs and GaSb materials systems of this work . . . 37
4.2 Total energy convergence of cubic GaX as a function of K-point MP-grid . . . 38
4.3 Computed the band gap of the calculated and experimental values of GaX(GaP,GaAs,GaSb) materials systems of this work . . . 40
4.4 Computed the lattice constant $a(\text{Å})$, the bulk modulus $B(GPa)$, formation energy $E_f(eV/atom)$, and the cohesive energies $E_{coh}(eV/atom)$ of selected graphene/ GaP,GaAs and GaSb materials systems of Heterostructure . . . 48
4.5 Cohesive Energies ($E_{coh}(eV/atom)$) versus equilibrium distance(d) GaP material systems of Heterojunction . . . 49
4.6 Cohesive Energies ($E_{coh}(eV/atom)$) versus equilibrium distance(d) GaAs material systems of Heterojunction . . . 49
4.7 Cohesive Energies ($E_{coh}(eV/atom)$) versus equilibrium distance(d) GaSb material systems of Heterojunction . . . 49
4.8 $E_f(eV)$ Vs equilibrium distance(d) GaP material systems of Heterojunction . . . 50
4.9 $E_f(eV)$ Vs equilibrium distance(d) GaAs material systems of Heterojunction . . . 50
4.10 $E_f(eV)$ Vs equilibrium distance(d) GaSb material systems of Heterojunction . . . 50
4.11 $Eperatom(eV)$ Vs equilibrium distance(d) GaP material systems of Heterojunction . . . 51
4.12 $Eperatom$ Vs equilibrium distance(d) GaAs material systems of Heterojunction . . . 51
4.13 $Eperatom$ Vs equilibrium distance(d) GaSb material systems of Heterojunction . . . 51
4.14 Computed the band gap of the calculated and experimental values of GaP, GaAs,and GaSb materials systems of heterostructures . . . 52
4.15 Absorption Energy of graphene/GaX(X=P, As, Sb) Heterostructure data . . . 53
4.16 ACF.data DFT output of Zinc-Blende(ZB) fo GaP . . . 55
4.17 BCF DFT output of Zinc-Blende(ZB) fo GaP . . . 55
4.18 AVF/data DFT output of Zinc-Blende(ZB) for GaP . . . 56
4.19 ACF.data DFT output of zinc-blende for GaAs . . . 56
4.20 ACF.data DFT output of zinc-blende for GaSb . . . 57

4.21 ACF hetero.data DFT output of graphene/GaP Heterojunction . . 57
4.22 ACF hetero.data DFT output of graphene/GaAs Heterojunction . . 58
4.23 ACF hetero.data DFT output of graphene/GaSb Heterojunction . . 58

Chapter 1

Introduction

Novel materials have been attracting great interest in materials science for more than two decades due to their unique electrical, optical, and mechanical properties. Varying novel materials with different characteristics are used to create semiconductors. The conductivity of these materials primarily lies between that of insulators and conductors. There are two types of semiconductors: direct band gap and indirect band gap semiconductors[1], which differ based on the position of energy in momentum space. In semiconductors with a direct band gap, the valence band's highest energy is directly above the conduction band's minimum energy in momentum space. While maintaining momentum, electrons at the conduction-band minimum can pair instantly with holes at the valence-band maximum. The momentum of the conduction band minimum and the indirect band gap semiconductors that straight transition across the band gap is not allowed since the valence band maxima are not the same. Group III-V semiconductors play a significant role in modern technology. They are becoming more crucial in numerous new applications for optoelectronic and electrical devices. The design of solid-state devices such as solar cell, light emitting diodes, photovoltaic cells, photo detectors, lasers, modulators, integrated circuits, filters, etc makes use of the valuable qualities of semiconductor materials[2] are a few examples of these uses, according to Jivani. For III-V semiconductors, numerous electronic band structure calculations have been performed. There are three of these: the full potential method[4], the empirical pseudopotential method[3], and the pseudopotential total energy approach[5]. To investigate the electrical and optical properties, we have presented the PAW computations of the band structures of pristine in GaX (X = P, As, Sb). A calculation of the exchange- correlation potential has been made. The generalized gradient approximation (GGA) and Perdew-Burke-Ernzerhof (PBE) [6] methods have been used to determine the total energy and the exchange- correlation potentials, respectively. The energy gaps vary widely in the semiconductor GaX (X= P, As, Sb), indicating that the energy band gap relies on how the band structure calculation is done[2, 4, 7, 8]. The band structure, density of states, electrical structures, and optical properties pristine of the semiconductor compound GaX (X= P, As, Sb) with a zinc-blende structure are all thoroughly calculated in this paper

They can be demonstrated that it is the ideal material for producing opt-electronic devices and solar cell economically. Thus, it can bee shown to be the best material for manufacture of optoelectronic devices and solar cell in economic mode.

Earlier, many efforts have been made to explore the linear and non-linear optical properties of different materials in the bulk state as well as in nanostate. It is zinc blend structured pristine possess strong visible emission around 589nm at room temperature and this material is used in early low brightness to medium based LEDs which generate different colors based on the addition of dopants. However, there are used in the manufacture of low-case red, orange and green light emitting diodes (LEDs) with low to medium brightness and semiconductor lasers can be made that emit in the visible spectrum, or even produce ultraviolet emission. It has a relatively short life at higher current and its lifetime is sensitive to temperature. The higher energy gap gives devices the ability to operate at higher temperatures, also used in power switching application semiconductor nanocrystals are tiny crystalline particles that exhibit size dependent optical and electronic properties. These particles also span the transition between small molecules and bulk crystal[9]. GaX(X=P, As, Sb)[10] is a III-V compound orange-red semiconductor material. The crystal structure pristine of gallium X(X= P,As,Sb) are spherical type and belongs to indirect transition semiconductors. As an important nonlinear optical crystal, GaX has attracted people's research interest. Rashid et al [11],studied the structure and electrical properties of GaX(X= P,As,Sb) by density functional theory. Liu Li [12] and others also studied the electronic structure, optical properties and anisotropy of GaX, providing theoretical basis for experimental research. We calculate the Raman scattering spectrum pristine of the GaX(GaP, GaAs, GaSb) crystal pristine compared with the experimental Raman spectrum values and gave optical permittivity [13]. It provides a theoretical basis for experimental research and practical application. Some of the atoms from group III of the periodic table combine with the atoms of group V to form III-V semiconducting compound, in a particular gallium phosphide (GaP), gallium arsenide(GaAs) and gallium antimonide (GaSb)semiconductor. Our calculations would show how the electrical and optical characteristics pristine of GaX compounds are affected when P is replaced by As and As by Sb. This paper's aim is to provide a comparative and complementary analysis of GPAW code implementation of the DFT method is used to examine electrical structures, electronics, and optical properties to both calculated and experimental values

1.1 Statement of the Problem

The statement of this thesis is to characterize alternate photovoltaic solar cell catalysts due to issues with the high cost of gallium and the gallium X compound's (X=P, As, Sb) vulnerability to carbon supported poisoning. We need highly efficient photovaltic solar cells, low-cost, light emitting diode(LED), transistors, photo cell, thermos-photovoltaic systems and dependable energy sources. Solar cells which directly convert sunlight into electricity are promising candidates for commercialization on a large scale. As a promising mechanism for the design of highly efficient solar cells, heterojunctions consisting of two types of donor and acceptor semiconductors were proposed. However, a high-quality graphene/GaX(X=P,As,Sb)Heterojunctions solar cell requires both donor. Semiconductor to have a direct band gap to absorb solar radiation, high carrier mobility

to promote efficient transportation of electrons, and high stability in ambient conditions. The dependency on donor and acceptor semiconductors makes it necessary to look for suitable materials with ideal band gap, high carrier mobility and high stability. Semiconductor to have a direct band gap to absorb solar radiation, high carrier mobility to promote efficient transportation of electrons, and high stability in ambient conditions. The dependency on donor and acceptor semiconductors makes it necessary to look for suitable materials with ideal band gap, high carrier mobility and high stability. Engineering the electronic properties of a material, specifically its band gap, is highly desirable for nano- and opto-electric applications and strain is one of the possible ways of doing so. They are very useful for flexible electronic and optoelectronic devices as well as for strain-engineered materials as possible. In solar cells there has to be effective electron-hole separation and such heavy separation of the charge not only facilitates the dissociation of excitons into free electrons and holes, but also greatly decreases the recombination rates of the electron-hole, which may lead to the long lifetime of the minority carrier. Photo-generated charging carriers must be separated within a photovolatic solar cell. Proper band alignment must be identified which is critical to the performance of solar cells. Because of their wide range of applications in catalysis, electrochemical energy storage, photocatalysis, electronics, optoelectronics, spintronics, and photonic nanodevices, two-dimensional(2D) materials have largely emerged to date. Given their fascinating properties, TMDCs have received considerable interest among these. However, the monolayers of the TMDCs display some drawbacks, such as large effective masses, poor dielectric screening, and strong excitonic effect, leading to the rapid rate of photon-generated electron and hole recombination. The short life span for the electron-hole pair results in extremely low quantum efficiency, thus drastically impeding the performance of the system.The stacking different 2D materials into layered vdW heterostructures is considered a realistic way to build applications of the next decade, ranging from nanoelectronics to optoelectronics and photonics, such as tunneling transistors, solar cells and bipolar transistors. Particularly in the layered vdW heterostructures, the formation of type-III-V band alignment is capable of modulating interlayer transition energy and responsible for charge separation, allowing intensive use of advanced optoelectronic devices in design.

1.2 Significance of the study

•The study's findings can be applied to the experimental design of photovoltaic solar cells by companies that manufacture photovoltaic solar cells
•Researchers working experimentally on unique aspects of graphene GaX(X= P,As,Sb) hetero junctions utilized in photovoltaic solar cell design will greatly benefit from the study
•The findings can serve as a starting point for future studies on the new features of graphene GaX(X= P,As,Sb) hetero-junctions used in photovoltaic solar cells

1.3 Objectives

1.3.1 General Objectives

The general objectives of this thesis is to investigate the first principles study of novel properties of pristine and carbon supported GaX (X=P, As, Sb) using Density function theory(DFT) within the implementation in GPAW open-source code.

1.3.2 Specific Objectives

The specific objectives of this thesis are:
•To identifying the electronic structures,electronic and optical novel properties of pristine and carbon supported GaX(X= P,As,Sb)
• To evaluate the stable and efficient heterostructure configurations for photovoltic and solar cell applications
•To calculate the band gap of GaX and compare the results with the experimental and computational values in the Zinc Belende pristine of GaX(X= P,As,Sb) structures
• To calculate the bulk modulus and optimaziation energy of GaX(X= P,As,Sb)
•To analyze and identfying the optical properties, absorption energy, formation and cohesive energy of graphene/GaX(X=P,As,Sb) heterostructure

1.4 Outline of the Thesis

This thesis is organized and separated into five chapters. Chapter one brief descrption about the background, statement of the problem, significance of the study, objectives and organization of the thesis. Chapter two described about the literature reviews descrption on DFT which allows us to accurately describe atomic geometry, electronic structure, electronic and optical properties,absorption energy of GaX(X= P,As,Sb)on graphene. Hence, we describe about ,Hamiltonian of Electronic system, Hartree-Fock Method, the Hartree Method, the Hohenberg-Kohn Theorem, the Exchange-Correlation Functional, pseudopotential method, the Kohn-Sham Equations, Local Density Approximation (LDA), Generalized Gradient Approximation (GGA), Hubbard-U scheme (DFT+U), the Bloch Theorem,Plane waves and Pseudo-potentials,Plane wave cut-off energy and K-points, analysis of the Electronic Properties, Charge Density, Geometry Optimization, which will be used to solve the DFT equations. Chapter three discusses implementation of DFT methodology. Chapter four brief descrption about the result and discussion of DFT output that depending on electronic structures,absorption, electronic and optical properties of all crystal structure of GaX(X= P,As,Sb), that is, cubic-zinc blende was reported and discussed that compared with experimental and computed results discussion. To obtain a further understanding the out put of DFT implementation. Chapter five concludes the results of the study and recommends for action and directs future research directions.

Chapter 2

Literature Review

2.1 Density Functional Theory

2.1.1 Introduction

First-principles methods based on density functional theory (DFT) are fundamental instruments for predicting the properties of materials in the field of materials science [18, 19, 20]. For a variety of material qualities, DFT can offer trustworthy and competent conclusions when compared to experimental data. On the other hand, DFT's strength lies in its capacity to predict changes in a material's properties. DFT can therefore help industrial designers foresee new materials with enhanced features. The basis theory in today's computational material science is DFT, which is widely applied. The computations on GaX(X=P,As,Sb) were completed by using density functional theory to the plane wave pseudo potential, Generalized Gradient Approximation (GGA), and Perdew Burke Ernzerhof (PBE). Although the many-body Schrdinger equation has the necessary physical knowledge, its practical use is constrained by our inability to identify a plausible explanation for the many-body effects that the exchange-correlation functional contains. Numerous exchange-correlation functional have been created recently and used successfully in simulation computations, [21]. Here, DFT offers a compelling substitute since it is a lot more adaptable and offers a mechanism to methodically map the many-body problem. In order to specifically look into the electronic structure of many-body hamiltonian systems, physics, chemistry, and materials science use a computational quantum mechanical modeling technique called density functional theory (DFT). The electronic structure of many-body systems, particularly atoms, molecules, and condensed phases, is studied using density functional theory (DFT), a computational quantum mechanical modeling technique. By employing functional (function of another function), which is specifically dependent on electron density $n(r)$, which is provided[22], one can use DFT to determine the parameters of a many-electron system. The electron density $n(r)$ is the fundamental quantity in the idea of density functional theory (DFT), and the discovery of DFT gave an efficient remedy. The electron density $n(r)$ is the central quantity in DFT

$$n(r) = N \int ... \int |\psi(r_1, r_2...r_N)|^2 dr_1 dr_2 ... dr_N \tag{2.1}$$

It is described as being the integral over all of the electrons' spin coordinates and over all but one of the spatial variables[23]. Where N is the system's total number of electrons. The reduction of the dimension from $3N$ to three spatial variables is the benefit of utilizing the DFT over the wave function. The density is always three dimensional, no matter how many electrons are present in the system. This makes it possible to apply DFT to systems with hundreds or even thousands of atoms. It establishes the likelihood that any of the N electrons will be present in the volume element $\vec{dr}$. The DFT just provides a one-electron potential in place of the unpredictable complexity of the interactions between electrons in the density of matter. This often indicates that the basic variable of the system depends solely on the three spatial coordinates x, y, and z rather than 3N degrees of freedom for N-electrons in a solid that obey the Pauli principle and repulse each other via the Coulomb potential. Density-functional theory (DFT), one of the most popular theoretical frameworks for electronic structure calculations, forms the foundation of GPAW[18, 24]. Additionally, time-dependent density-functional theory (TD-DFT)[25] is used. We employ the projector augmented wave (PAW) method[26], which is implemented using uniform real-space grids and finite differences, for numerical approximations. Additionally available is an alternative atomic orbital basis set. As we focus here on the Python related implementation issues, we use only the real-space grid based standard ground state DFT to illustrate the important aspects. GPAW is an integrated suite of Open-Source computer codes for electronic-structure calculations and materials modelling at the nano-scale. It is based on density-functional theory, projector agumented plane waves(PAPW), atomic simulation enivromental(ASE), and pseudo-potentials. It does not aim at providing a single monolithic code able to perform several different tasks by specifying different input data to the same executable. Interoperability of different components within GPAW is granted by the use of common formats for the input, output, and work files

2.1.2 Hamiltonian of Electronic system

The main tools to handle the physical chemistry for micro systems are provided by the invention of quantum mechanics by "Heisenberg, Schrdinger," and many other brilliant scientists. The given non-relativistic physical system is described using the time independent Schrdinger equation. It has the following form:

$$\hat{H}\psi = E\psi \tag{2.2}$$

Where $\hat{H}$ represents the Hamiltonian operator which describes the way that particles interact with one another, and ψ is the wave function and E is energy of the particular state of a system, respectively. To solve first principle theory for a sytem of nuclei and electrons, the many-body Schrodinger equation is used. The many-body Schrodinger equation is given as follows:

$$\hat{H}\psi(R_I, r_i) = E\psi(R_I, r_i) \tag{2.3}$$

Where $\hat{H}$ is the Hamiltonian of the system and E is the total energy, $\psi(R_I, r_i)$ is the many-body wavefunction describing the state of the system, R_I andr_i are the positions of ion I and electrons i. In general the many-body Hamiltonian $\hat{H}$ for a system of electrons and nuclei can be expressed as:

$$\hat{H}(R_I, r_i) = T_e(r_i) + T_N(R_I) + V_{NN}(R_I) + V_{ee}(r_i) + V_{Ne(r_i,R_I)}$$

(2.4)

$$\hat{H} = -\frac{\hbar^2}{2M_I}\sum_I \nabla_I^2 - \frac{\hbar^2}{2m_i}\sum_i \nabla_i^2$$

$$+ \quad \frac{1}{2}\sum_I \frac{Z_I Z_J e^2}{|R_I - R_J|} - \sum_{Ii} \frac{Z_I e^2}{|R_I - r_i|} + \frac{1}{2}\sum_i \frac{e^2}{|r_i - r_j|}$$

Where $\hbar$ is the Planck's constant divided by 2π ($h = \frac{\hbar}{2\pi}$), e is the electron charge, Z_I is the charge of the nuclei, M_I is the mass of I^{th}nuclei, m_i is the mass of ith electron. Therefore,the contribution to the hamiltonian come from the kinetic energy T of nuclei and electron and the potential energy due to the Coulomb interaction of nuclei-nuclei ($V_{IJ=NN}$), nuclei-electron $V_{ext=Ne}$ (External potential) and electron-electron (V_{e-e}), respectively

2.1.3 The Hartree Method

In 1927 two years after the Schrodinger equation was published Hartree proposed method of solving this equation for multiple electron systems. Hartree assumed that each electron moves in the average potential of the electrostatic interactions with surrounding electrons suggested independent electron approximation. This is rewrite as a one-particle equation for an electron moving in an average potential from all the electrons, as proposed by Hartree. The wave function then becomes:

$$\psi(r_1, r_2, ...r_n) = \Phi_1(r_1)\Phi_2(r_2)...\Phi_n(r_n) \tag{2.5}$$

Where $\Phi_i(r_i)$ are independent of wave function. This expression is a Hartree product and this function is not antisymmetric. An antisymmetric wave function can be mathematically described as follows:

$$\Psi(r_1, r_2, ...r_j, ...r_k, ..., r_n) = -\Psi(r_1, r_2, ...r_k, ...r_j, ..., r_n) \tag{2.6}$$

Thus Hartree method did not respect the principle of antisymmetry of the wave function (Hartree product does not satisfy the Pauli principle)[27]

2.1.4 Hartree-Fock Method

In 1930 Fock applied Slater determinant to the Hartree method and proposed that the Hartree Fock method. Electrons being fermions (Pauli principle), the exact many-particle wave function needs to be anti-symmetric by exchange of electrons (the sign of the wavefunction becomes opposite for the exchange of electrons) as shown in Equation (2.6). For simplicity let us consider the exchange of electrons in the case of two electron atom as an example

$$\Psi(r_1, r_2) = \frac{1}{\sqrt{2}}[\Psi(r_1, r_2) - \Psi(r_2, r_1)] = -\Psi(r_2, r_1) \tag{2.7}$$

Where $\frac{1}{\sqrt{2}}$ is the normalization constant

$$\Psi(r_1, r_2) = \frac{1}{\sqrt{2}}\Phi_1(r_1)\Phi_2(r_2) - \Phi_1(r_2)\Phi_2(r_1) \tag{2.8}$$

The antisymmetric wavefunction in Equation(2.7) can be written as a determinant

$$\Psi(r_1, r_2) = \frac{1}{\sqrt{2}} \left| \begin{bmatrix} \Phi_1(r_1) & \Phi_1(r_2) \\ \Phi_2(r_1) & \Phi_2(r_2) \end{bmatrix} \right.$$

(2.9)

For the case of N electrons, the antisymmetric wavefunction can be described in a determinant form:

$$\Psi_(r_1, r_2 ... r_N) = \frac{1}{\sqrt{N!}} \left| \begin{bmatrix} \Phi_1(r_1) & \Phi_1(r_2) & \dots & \Phi_1(r_N) \\ \Phi_2(r_1) & \Phi_2(r_2) & \dots & \Phi_2(r_N) \\ \vdots & \vdots & \ddots & \vdots \\ \Phi_N(r_1) & \Phi_N(r_2 & \dots & \Phi_N(r_N) \end{bmatrix} \right.$$

(2.10)
This determinant is called the Slater determinant. Equation (2.10), is Hartree-Fock approximation; that insures the electrons are indistinguish-able and therefore associated with every orbital

2.1.5 Born-Oppenheimer Approximation

Cosider a molecule with N nuclei at $R_1, ..., R_N \equiv R$ and N_e electrons ($r_1, ..., r_{Ne}$) in Born-Oppenheimer approximation, the wave functions of electrons are only determined by the positions of atomic nuclei, therefore the kinetic terms in Eq.(2.13) can be treated separately. The equation of electronic motion can be described as:

$H_e\psi_e(r, R) \equiv E_e\psi_e(r, R)$ (2.11)

. where ψ_e is the wavefunctions of electrons, and H_e represents the Hamiltonian of electrons. The later can be further described as:

$$H_e = T_e(r_i) + V_{ne}(r_i, R_I) + V_{ee}(r_i) \tag{2.12}$$

In addition, the equation of atomic nuclei motion is described as:

$$H_N\psi_N(r, R) = E_N\psi_N(r, N) \tag{2.13}$$

Where ψ_N is the wavefunctions of atomic nuclei, and H_e represents the Hamiltonian of atomic nuclei. The later can be further described as:

$$H_N = T_N(R_I) + V_{NN}(R_I) + E_e \tag{2.14}$$

In particular Equation (2.12) can be expressed as:
Kenetic Energy:

T$_e = -\frac{1}{2}\sum_{Ne}^{i=1} \nabla i^2$ (2.15)

Electron-Electron Repulsion:

V$_{ee} = \sum^{ij} \frac{1}{r_i - r_j}$ (2.16)

External-Potential:

$$V_{ext} = -\sum_{i=1}^{Ne}\sum_{i=1}^{N} \frac{Z_I}{|r_i - R_I|} = \sum_{i=1}^{Ne} V_{ext}(r_i, R) \tag{2.17}$$

Total Molecular Hamiltonian:

H = H$_e + T_e + V_{NN}$ (2.18)

$$T_N = -\sum_{I=1}^{N} \frac{1}{2M_I}\nabla_I^2 \tag{2.19}$$

$$V_{NN} = \sum_{I,I>J} \frac{Z_I Z_J}{|R_I - R_J|} \tag{2.20}$$

The Born-Oppenheimer approximation does not describe the motion of the atoms straightforward, which is quite different with the classical Newtonian mechanics. The time independent, non-relativistic Schrodinger equation can be solved accurately for one-electron system. While for complex systems containing more than one electrons, the electrostatic interactions between those electrons are more complicated

2.1.6 The Hohenberg-Kohn Theorem

This theorem was born in 1964 with the paper of Hohenberg and Kohn. Modern theory presented the principles of DFT is based on the two Hohenberg-Kohn (HK) theorems[28]. The ground density of state $n_o(E)$ describes the wave-function of the electrons. The density of state $n(E)$ is defined as the number of electrons per volume at the point r in space
The density is normalized to the number of electrons.

$$N = \int n(r)dr^3 \tag{2.21}$$

The energy and density of the suitable ground state can be estimated theoretically. The two theorems are as follows:
Theorem 1: States that if there are N interacting particles in a system and they are moving in an external potential $V_{ext}(r)$, the $V_{ext}(r)$ is uniquely determined by the ground state particle density $n_o(E)$; so the total energy is a unique functional of the electrons density

$$E_{HK} = E[n(r)] = T[n] + E_{int}[n] + \int V_{ext}(r)n(r)dr \tag{2.22}$$

Where E_{HK} is the total energy, $T[n]$ is the kinetic energy and $E_{int}[n]$ is the part coming from the electonic interaction.

$$E_{HK}[n] = F_{HF}[n] + E_{ext}[n] \tag{2.23}$$

Where $F_{HF}[n]$ is a universal functional of the electron density $n(r)$ and $E_{ext}[n]$ is the interaction energy with the external potential
Theorem 2: This states that the electron density which minimizes the energy of the over all functional is the the electron ground state density $n_o(r)$ and the minimum energy is the ground state energy(E_o): [29]

$$minE_{HK}[n] = E[n(r)] = E_o < E_{HK} \tag{2.24}$$

2.1.7 The Kohn-Sham Equations

In 1965, Kohn and Sham published a paper which transformed density functional theory(DFT) into a practical electronic structure theory. Kohn and Sham dealt with the original problem of a many-body system of interacting particles by mapping it into another problem of non-interacting electrons of the same density $n(r)$. Therefore, it can be explained as the total energy functional of a non interacting particle system subject to two potentials: the external potential and an exchange correlation potential,V_{ext}. Therefore, the independent single-electron Kohn-Sham equations can be written as:

[- $\frac{\hbar^2}{2m}$ $\nabla_i^2 + V_{ext}(r) + V_H + V_{xc}]\psi_i = \varepsilon_i\psi_i$ (2.25)

Where ε_i are the eigenvalues of the hypothetical KS particles. The highest laying eigenvalue defines the chemical potential for electrons (Fermi level) and it is the only quantity which has a well defined physical interpretation. The independent-particle wave function only depends on the effective potential V_{eff} and ε_i. Where V_{eff} are the effective potential that defines the interaction between electron and nuclei,when V_{ext} is the external potential, V_H is the Hatree potential and V_{xc} is the exchange-correlation potential and defined thus

$$V_H = \int \frac{n(r)}{r-r'} dr'^3 \tag{2.26}$$

and V_{xc} is the potential that defines the exchange and correlation contribution and is the derivative of the exchange-correlation energy:

$$V_{xc} = \frac{\delta E_{xc}(r)}{\delta n(r)} \tag{2.27}$$

From the Hohenberg-Kohn variational principle, the ground-state density $n(r)$ corresponding to the external potential V_{ext} can be obtained as solution of the Euler equation as:

$$\frac{\delta E_H[n]}{\delta n(r)} = \frac{\delta F[n]}{\delta n(r)} + V_{ext}(r) = 0 \tag{2.28}$$

The exact ground-state density of a N-electron system by construction is defined by:

$$n(r) = \sum_i^N |\Psi(r)|^2 = \sum_i^2 n_i(r) \tag{2.29}$$

Where $n_i(r) = |\Psi(r)|^2$ is the density of single particle. According to Eq. (2.30), the total energy functional can be expressed by Hohenberg-Kohn theorem in terms of the independent particle wave function:

$$E_{HK} = \langle\Psi|\hat{T}\Psi| + \frac{1}{2}\int\int \frac{n(r)n(r')}{|r-r'|} dr dr' + \int V_{ext}(r)n(r)dr + E_{xc}[n]$$

$= \mathrm{T}_s[n] + E_H[n] + E_{ext}[n] + E_{xc}[n](2.30)]$
Where $T_s[n]$ is the independent particle kinetic energy,$E[n]$ is the Hartree energy due to the interaction between the electrons and $E_{xc}[n]$ is the exchange-correlation energy which includes all the quantum mechanical effects. Comparing the Hohenberg-Kohn equation(2.26), the exchange-correlation energy can be written as

$$E_{xc}[n] = F_{HK}[n] - (T_s[n] + E_H[n]) = (T[n] - T_s[n] + (E_{e-e[n]} - H[n]) \tag{2.31}$$

Unfortunately, because the form of the kinetic energy functional is still unknown, the minimum of the total energy functional could not be determined directly. Furthermore, neither the true form ofE_{e-e} nor the true form of the exchange-correlation energy functional is known. Kohn and Sham proposed a viable way to solve this problem, the so-called Kohn-Sham scheme. Accordingly, all other variables (including the leftover kinetic energy) are incorporated in the so-called effective or Kohn-Sham one-electron potential. Therefore, the independent single-electron Kohn-Sham equations can be explained on the above equation (2.32). The DFT solution for a single independent-particle system can be understood as a question of ground state electronic energy minimization. Actually, in Eq.(2.31), the kinetic energy T_s can be expressed as a functional of the orbitals $\Psi_i(r)$ and the other terms (E_H, E_{ext}, E_{xc}) are functional of the density n

2.1.8 Variational Principle

The variational principle is a theorem used to systematically determine the ground state wave function,ψ_o and its energy. It states that the calculated energy for an arbitrary wavefunction is always larger than the ground-state energy, can be used to determine the ground-state wavefunction[?]. In the solution of the Schrodinger equation, the number of electrons,N and the potential of nuclei, V_{n-e}, for certain material are the system dependent parameters. Hence the wavefunctions,ψ and the corresponding eigenvalues of the electronic Hamiltonian, $\hat{H}$ can be determined

$$\hat{H} = -\frac{1}{2}(\sum_{i=1}^{n} \nabla_i^2) + \sum_{i=1}^{n} V_{ext}(r_i) + \sum_{j} \sum_{i>>j} \frac{1}{r_{ij}} \tag{2.32}$$

.

2.1.9 The Exchange-Correlation Functional (E$_{xc}$)

The Kohn-Sham formalism is exact with the assumption that the exchange correlation functional $E_{xc}[n(r)]$ is known. However, in principle no analytical form of this functional exist, hence computations often rely on approximations. The reliability of the DFT calculations hugely depend on the parametrization scheme adopted for the exchange-correlation. Since the birth of DFT some sort of approximations for E_{xc} have been used. The simplest physical ways to approximate E_{xc} are Local-Density Approximation (LDA), Generalized Gradient Approximation(GGA); Perdew-Burke-Ernzerhof(PBE), Hybrid functional and Hubbard-correction (DFT+U).[27, 28, 30, 29, 48].

(a) Local Density Approximation (LDA)

The local density approximation (LDA) is one of the common approximation to the exchange-correlation functional. This approximation uses the homogenous interacting electron gas to model the exchange correlation functional. In general,

the LDA over-estimates the binding energies and underestimated band-gap energies. Strictly, the LDA is valid only for slowly varying densities[31].The exchange-correlation potential at each position is known.

$V_{xc} = V_{xc}^{homo}[n(r)]$ (2.33)

. The LDA is an approximation for the exchange-correlation energies(E_{xc}) of homogeneous electron gas which can be defend as

$E_{xc}^{LDA}[\rho(r)] = \int \rho(r)\varepsilon_{xc}^{homo}(\rho(r))dr$ (2.34)

Where $\varepsilon_{xc}^{homo}$is the exchange-correlation energy density per volume unit(particle of the homogeneous electron gas of density $\rho(r)$ and is expressed as sum of two components as two parts.

$E_{xc}^{LDA} = E_{x}^{LDA} + E_{c}^{LDA}$ (2.35)

Many systems, such as bulk metals, benefit from LDA because the electronic density is nearly uniform. However, there is an evident restriction to LDA, which is that it may fail in systems with inhomogeneous electrical density. As a result, the better approximations should be built. In LDA, the exchange-correlation energy of each element only depends on the local electron density at that element. However, the exchange-correlation energy does not include the non-local contributions resulted from the in-homogeneities in the real electron density at a distance from the element

(b) Generalized Gradient Approximation (GGA)

LDA fails to predict exact-exchange energy when its density undergoes rapid changes such as for true electron density. Improvements, especially of the convergence and for the binding energies, came up with the generalized gradient approximationGGA) by Pedrew[27, 6].The gradient approximation corrects the exchange-correlation potential of the LDA by a Taylor expansion of the position variables of the gradient of the electron density $\nabla\rho(r)$: then,the exchange-correlation energy can be written by the following form;

$$E_{xc}^{GGA}[\rho(r)] = \int \rho(r)\varepsilon_{xc}^{GGA}(\rho(r)))\nabla\rho(r)dr \qquad (2.36)$$

Where $\nabla\rho(r)$ is gradient of density at each coordinate. The advantages of the

GGA are the more precise binding-and atomisation energies.The gain of exactness demands the time-consuming computation of the density gradients. In GGA, the electron density, as well as the gradient of density, are found in the exchange-correlation functional. The GGA is perfect for a system that contains very high electron density, in which the exchange-correlation energy is the key feature

PBE

The PBE exchange-correlation functional can be expressed as

$$E_{XC}^{PBE} = \int n\varepsilon_X^{LDA}(n)F_{XC}^{PBE}(r_s, S) \tag{2.37}$$

Where $F_X^{PBE}(s) + F_C^{PBE}(r_s, S)$ denotes the PBE enhancement factor.PBE functional satisfies some conditions,such as the inhomogeneous electron gas.Theoretically,GGA PBE provides more accurate features than LDA.For PBE exchange functional,the enhancement factor is given by

$$F_X^{PBE}(S) = 1 + K - \frac{K}{1 + \frac{\mu}{K}S^2} \tag{2.38}$$

.

(c) Hybrid Functional

Hybrid functionals mix the Hartree-Fock exchange integral with GGA exchange functionals at a constant ratio, which makes the Kohn-Sham energies of the independent electron model link to those of the fully interacting electron one. That is, hybrid functionals are constructed by connecting exchange functionals, which are assumed as the exchange energies of the independent electron systems, to the Hartree-Fock exchange integral, which are taken as the exchange energies for the fully interacting systems. The Heyd, Scuseria, and Ernzerhof(HSE) hybrid functional extends the PBE exchange correlational functional by mixing the Hartree-Fock exchange integral only for the short-range part[32] . The Lack of long-range exchange interactions is one of the major problems of GGA exchange functionals. However, the long-range correction for GGA exchange functionals yields much larger high occupied molecular orbitals (lower energy)-lower unoccupied molecular orbitals (higher energy) gaps for semiconductors than the corresponding experimental band gaps, mixed in the GGA exchange functionals high occupied molecular orbitals-lower unoccupied molecular orbitals gaps calculated approaches the experimental band gaps in semiconductors and should be calculated intrinsically in excited state calculations such as time dependent Kohn-Sham calculations. The exchange potential employed in HSE is divided into short-and long-range parts, and HF exchange is mixed with Perdew-Burke-Ernzerhof(PBE) exchange in the short-range part[48]. Break HSE is a range-separated hybrid functional, which splits the exchange term into short-range (sr) and long-range (lr) parts to avoid the demanding integrals over the long-range part of exact exchange as expressed in Equation (2.39)

$$E_{xc}^{HSE} = aE_x^{HF,sr}(\mu) + bE_x^{PBE,sr}(\mu) + E_x^{PBE,lr}(\mu) + E_c^{PBE} \tag{2.39}$$

. Where short-range(sr) and long-range(lr) refer to the short-range and long-range parts of the respective exchange interactions, and is the parameter that defines the range separation of the Coulomb kernel which varies between $0.2A^o$ and $0.3A^o$ Hence HSE was made by fock mixing parameter $a = 25\%$ exact exchange with $b = 75\%$ of PBE (Perdew-Burke-Ernzerhof formulation of GGA) exchange. The HSE functional yields excellent results, in molecules and solids, for many different properties HSE functional is represented as:

$$E_{xc}^{HSE} = aE_X^{HF,sr} + (1-a)E_x^{PBE} + E_c^{PBE} \tag{2.40}$$

Where $E_x^{HF,sr}$ is the short-range part of the Hartree-Fock exchange integral and $a = \frac{1}{4}$. The hybrid functionals are computationally demanding, which prohibits their application to large system of atoms

(d) Hubbard-correction(DFT+U)

The basic idea behind DFT+U is to treat the strongly correlated electronic states of a system (typically, localized d or f orbitals) using the Hubbard model, while the rest of valence electrons are treated at the level of standard approximate DFT functionals. In the Hubbard model, the electron-electron repulsion of electrons on a site atom of a metal is quantified by the on site-Hubbard parameter U. In band structure calculations, such a scheme ensures separate treatments for highly localized d or f electrons and less localized s and p electrons. Within DFT+U the total energy of a system can be written as follows[33]

$$E_{DFT+U} = E_{DFT} + E_U \tag{2.41}$$

where E_U is the term that contains the Hubbard Hamiltonian to model correlated states (Hubbard correction energy):

$$E_U = \frac{1}{2}\sum_{I,m,m'\delta}(U^I - J^I)(\delta mm' - n_{mm'}^{I\delta})n_{mm'}^{I\delta} \tag{2.42}$$

Where $(U^I J^I)$ is effective Hubered parameter (U_{eff}) ,$n_{mm'}^{I\delta}$ is the occupation matrix and given by

$$n_{mm'}^{I\delta} = \sum_{\mu,\kappa} f_{\mu\kappa}^{\delta}\langle\Psi_{\mu}^{\delta}\kappa|\Psi_{m'}^{I}\rangle\langle\Psi^{I}_{m\}|\Psi_{\mu}^{\delta}\kappa\rangle}(2.43)$$

and the total occupation localized state (d or f) at site I is

$$n^I = \sum_{m,\delta} n_{mm'}^{I\delta} \tag{2.44}$$

.

2.1.10 The Bloch Theorem

To do DFT calculations on infinite systems, one must first assume that the systems structure is homogeneous in all directions and then apply periodic boundary conditions (pbc). We introduce a supercell for the set of coordinates of atomic nuclei, which involves a periodically repeating pattern of atoms fulfilling translational symmetry criteria. The Bloch theorem [34] states that the eigenvalues in a periodic solid have the form:

$$\Psi_{nk}(r) = \varrho^{ikr} u_{nk}(r) \tag{2.45}$$

Where n is the "band index" and k is a wave vector confined to the first Brillouin zone of the reciprocal lattice. u_k is translationally invariant, and they are obtained by

$$u_{nk}(r+T) = u_{nk}(r) \tag{2.46}$$

where T is a translational vector of the crystal lattice. Eigenstates of this form are called Bloch functions. Wave functions Ψ_{nk} and their eigenvalues are periodic in k-space,

$$\Psi_{n,k} + G(r) = \Psi_{nk}(r)E_{n,k} + G(r) = E_{nk}(r) \tag{2.47}$$

where G is an arbitrary reciprocal lattice vector. Hence it is sufficient to consider them and their eigenvalues only in the first Brillouin-zone. Deriving the Schrodinger equation with Bloch functions yields an equation for a periodic function $\Psi_k(r)$. Using periodic boundary conditions leads to a Hermitian eigenvalue equation over the Wigner-Seitz cell in the crystal. For a fixed k, there is an infinite number of solutions with rising energy values

2.2 Crytal Structure of GaX (X=P, As, Sb)

A lattice parameter can be used to describe the structure of all crystals. Recently, the local density approximation was used to represent GaX(X=P,As,Sb) within density functional theory (DFT) (LDA). The zinc-blende structure(ZB)GaP,GaAs,and GaSb compounds have the lowest minimum total energies. At atmospheric pressure, it is the most stable phase of these compounds. When pressure is applied, the volume decreases and, at relatively low pressure, a transition to the phases of the rocksalt (NaCl) and wurtzite structures occurs, with the znic-blende structure being more stable than the other. When attempting to learn more about the many characteristics of the class of binary compounds under pressure, this observation is intriguing. The GPAW approach, which was suggested to assess the electron phonon scattering time and provide insight into electronic de-excitation by intervalley phonons, was used to determine the phonon density of states (PDOS).The GaX(X=P,As,Sb) structural and electrical characteristics were examined using the DFT, and the lattice parameters, bulk modulus and pressure derivative, formation energy, and cohesive energy per unit cell were compared to Early values. According

to Garcia and Marvin, the transition from the zinc-blende (ZB) structure to the rocksalt (RS) structure took place at 18.8 GPa and the RS structure. Depending on the pressure being applied, the cubic zinc-blende (B3) and cubic rocksalt (or Rochelle salt) crystal structures that GaP,GaAS and GaSb shares are B3 and B1, respectively. Figure 2.3 illustrates this organization in schematic form. The cubic zinc blend form is where the majority of groups III-V compound semiconductors crystallize. The cubic zinc blende structure is present in the compounds gallium phosphide (GaP), gallium arsenide (GaAs), and gallium antimonide (GaSb). Each atom is located in the center of a regular tetrahedron, which has atoms of the opposite kind at each of its four corners

(a) Zinc-blende structure of GaP, GaAs, and GaSb

It is only possible to stabilize the metal stable cubic zinc-blend structure on cubic substrates like GaP, GaAs, and GaSb by heteroepitaxial development. According to calculations using the current abinitio method, the calculated lattice constants for the zinc blende poly type of GaP, GaAs, and GaSb are expected to be 5.54 Å with 5.45 Å, 5.65 Å with 5.76 Å, and 6.10VÅ with 6.21 Å. The cubic zinc-blend structure has two interpenetrating face-centered cubic (fcc) sub lattices that are shifted along the body diagonal by one-fourth of the length of the body diagonal, according to the symmetry described by space groups $F\bar{4}3m$ in the Hermann-Gauguin notation and Td^2 in the Schoenflies notation [35, 36, 37]. The main difference between the structures of wurtzite and zinc blende is the bond angle of the second-nearest neighbors and, consequently, the stacking order of closely packed diatomic planes. With the exception of the two different types of atoms occupying alternate positions in the lattice, the cubic zinc blende structure's unit cell is identical to that of the diamond form. The two sub-lattices are separated from one another by a fourth of the cube's body diagonal. Due to its lack of a center of symmetry, the cubic zinc mix structure is one of the most basic crystals and is therefore capable of exhibiting pizeoelectric and related properties that depend on polar symmetry. The distance between the lattice points of the basic cubic refrence lattice is known as the lattice constant a. The experimental value of the lattice constant "a" for gallium phosphide (GaP),gallium Arsenide(GaAs),and gallium antimonide(GaSb) are 5.4505Å,5.65Å,and 6.10Å whereas the value determined by these study were 5.54Å, 5.76Å and 6,21Å. When impurity atoms are added, the lattice constant of a semiconductor might change. One of the simplest and most crucial parameters is crystal density. A zinc blend lattice unit cell contains four molecules for each compounds

(b) Rocksalt structure of GaP, GaAs, and GaSb

High-pressure phase transition from the wurtzite to the rocksalt structure decreases the lattice constant down to the range of $4.271 - 4.294$. The space group symmetry of the rocksalt type of structure is $Fm3m$ in the Hermann-Mauguin notation and O_h^7 in the Schoenflies notation, and the structure is sixfold coordinated. However, the rocksalt structure cannot be stabilized by the epitaxial growth[36]

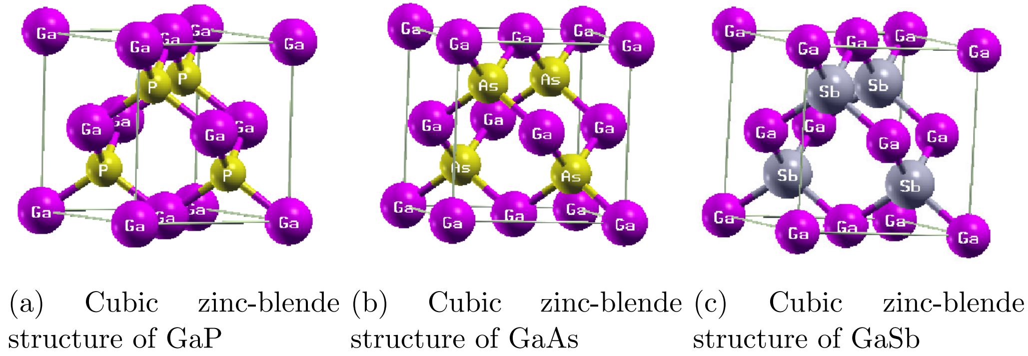

(a) Cubic zinc-blende structure of GaP (b) Cubic zinc-blende structure of GaAs (c) Cubic zinc-blende structure of GaSb

Figure 2.1: Cubic zinc-blende structures of GaX

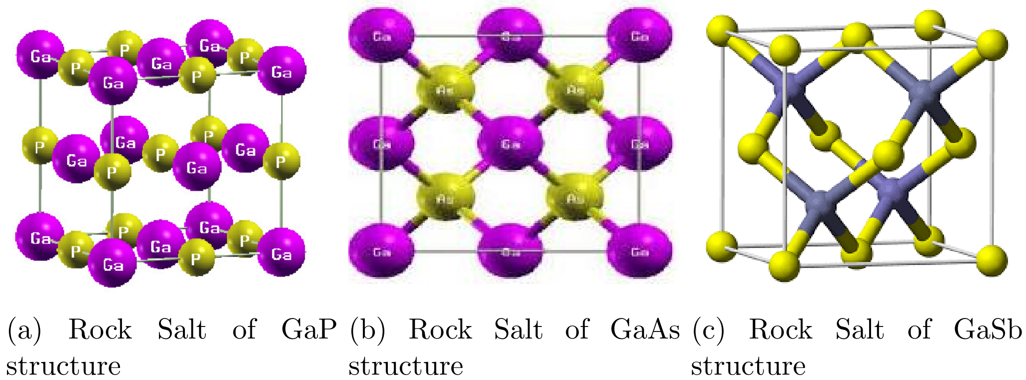

(a) Rock Salt of GaP structure (b) Rock Salt of GaAs structure (c) Rock Salt of GaSb structure

Figure 2.2: Crystal structure of GaX

Phase diagram

With the second harmonic generation (SHG) approach, the pressure-induced $B4-B1$ structural phase boundaries of GaX(GaP,GaAs, and GaSb) may be identified at high temperature. GaP has a phase boundary with an approximately $300K/GPa$ between $22.2GaP$ and $27GPa$ and $27K/GPa$ below $5eV/GPa$. The GaP initially has a cubic Zinc-blende structure that changes into a rocksalt structure at high pressures[38]. At temperatures around 900 K, the transition pressure drops to 22.2GPa and exhibits significant hysteresis, according to research from Russia. This is because the cubic zinc-blend-to-rocksalt phase transition exhibits substantial hysteresis at temperatures of $300K$ 22.2Gpa on compression and ~ 2 Gpa on decompression). The function of the atoms' Bader charges is shown on the horizontal axis,(x)[39] .Phase separation at low temperatures is anticipated by the phase diagram

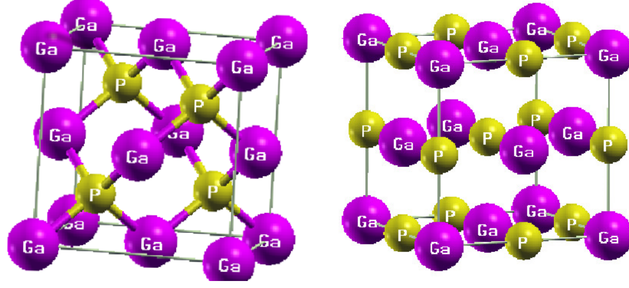

(a) Cubic Zinc-blende of GaP-B3 structure (b) Rock Salt of GaP-B1 structure

Figure 2.3: Crystal structure of GaX

2.2.1 The Electronic Properties of GaX (X=P, As, Sb)

Computational materials science gives researchers a powerful tools for examining electronic structure and properties. A couple of these will be discussed below, particularly the density of states and charge density analysis.

Density of States (DOS) and Band Structure

Density of States(DOS)

The density of states (DOS) describes number of states per unit of energy E (and per unit of volume in extended matter) is an essential property for many applications[40]

$$\begin{aligned} n(E) &= \frac{1}{N_k} \sum_i \sum_k \delta(\varepsilon_{i,k} - E) \\ &= \frac{\omega_{cel}}{2\pi^d} \int_{BZ} \delta(\varepsilon_{i,k} - E) dk \end{aligned}$$

In the case of independent-particle states, $n(E)$ from Equation (2.48), is the number of independent particle states per unit energy, where as $\varepsilon_{i,k}$ represents the energy of an electron (or phonon). In theory, calculating the integral in Eq.(2.48) is not a simple operation. The linear tetrahedron technique (LTM) by Jepsen and Andersen[41], the modified tetrahedron approach (MTM) by Bloch et al.[42], and the Gaussian broadening method (GBM) by Methfessel and Paxton [43] are three common types of methods for this Brillouin zone integration. The latter is being used in this thesis work. The projected density of states (PDOS) is defined by:

$$n(\alpha, E) = \sum_i \sum_k |\langle \Psi_{\alpha k}(r) | \Psi_{ik}(r) \rangle|^2 \delta(\varepsilon_{i,k} - E) \tag{2.49}$$

. where $\Psi_{\alpha k}$ denotes orthonormal states to Ψ_{ik} . The PDOS is a DOS projection onto atomic orbitals, in principle. At absolute zero temperature, the Fermi Energy E_F is the energy of the highest occupied quantum state in a system of fermions. Because the Fermi energy E_F appears in all DOS / PDOS spectra, it is often

intentionally made to coincide with the zero energy level by shifting the energy levels from E to $E - E_F$. Band structure is the plot of the energies of electrons eigenvalue energies (k) against the k points

Band Strucutures

Band structures are a representation of the allowed electronic energy levels of solid materials and are used to inform their electrical properties. A band structure is a 2D representation of the energies of the crystal orbitals in a crystalline material. Sometimes referred to as spaghetti diagrams, a band structure pristine plot can quickly reveal whether a material is metallic, semi-metallic, or insulating, and for those materials with band gaps whether they are direct or indirect as well as the magnitude of the gap. Additionally, the curvature of the bands can reflect the carrier mobility through those bands. For a material with an even number of electrons per unit cell and a large gap ($E_g \geq 3eV$) between the highest filled state and the lowest empty state, an insulating crystal results. The application of a modest electric field cannot alter the electron distribution function because to do so would require a large energy E_g [44]. A material which is insulating at low temperature, but whose band gap E_g is small ($0.1eV \leq E_g < 3eV$) is called a semiconductor. At finite temperature a few electrons will be excited from the filled valence band to the empty conduction band. These electrons and holes can carry current. Because the concentration of electrons in the conduction band varies like $\frac{EG}{e^{2k_BT}}$, the conductivity increases with increasing temperature[44, 45]. When the highest band is only partially filled, one has a metal. There are other issues, however. Band overlapping can complicate matters and cause elements to form metals, as can the Mott transition (qv) due to electronelectron interactions

Band Gap

The valence band and the conduction band are the two distinct areas of the DOS. The band gap is a region of energy that divides the valence and conduction bands and includes no electronic states at all. If the band gap is "small" that implies greater than 0.6eV to 3eV, materials are categorized as semiconductors. If the band gap is "wide" materials are classified as insulators. The distinction between these two types of materials is arbitrary, however band gaps greater than $3eV$ are commonly referred to be wide band gaps.The band gap is less than 0.5/0.6eV are metals materials possessing a non-zero DOS at the Fermi level.
The calculated values of band gaps pristine of GaP, GaAs and GaSb have ZB structure are 2.41 eV, 1.34 eV and 0.92 eV respectively and for Rocksalt structure 2.29 eV, 1.02 eV and 0.66 eV respectively. Some experimental values of band gaps of GaP, GaAs and GaSb have ZB structure are 2.26eV, 1.42eV and 0.73eV and for Rocksalt structure are 2.24 eV, 0.72 eV and 0.65 eV respectively. Therefore,the result of GaP > GaAs> GaSb that implies 2.41 eV > 1.34 eV > 0.92 eV

Charge Density

Charge density ($\rho(r)$) is defined as the amount of charge contained within a certain volume divided by the volume. It is related to the number charge density, also called the electron density ($n(r)$). Because it depends on the position vector r, it is a spatial charge distribution over the volume of a molecule or a unit cell of a periodic solid in quantum mechanics. The electronic charge density is thus given by the equation:

$$\rho(r) = e \sum_{nk} |\Psi_{nk}(r)|^2 = en(r) \tag{2.50}$$

Where, e is the electrons charge ($e = 1.6021733 \times 10^{-19}$ Coulomb),$\Psi_{nk}(r)$ is the nth bands wave function, and the sum extends to over all occupied electronic states. The electron density can be visualized by plotting 3D isosurfaces (a surface for a discrete isovalue) or 2D contour plots (a set of isocontours)

2.2.2 Geometry Optimization

Finding the system's electronic ground statethe precise configuration of atoms that corresponds to the lowest potential energyis essential for performing ab-initio calculations. When searching for the ideal arrangement of atoms,the quantum-mechanical code undertakes several ionic relaxation steps, which involves moving all of the nuclei in the proper direction (along energy gradients) such that each nucleus has a lower potential energy. After each ionic step,a self-consistent cycle of electronic relaxation stages must be employed to calculate the ground state energy.When the energy gradients (or forces on atoms) are smaller than pre-defined tolerance values,the geometry optimization process stops a final self-consistent cycle of the electronic relaxation must be employed to calculate the ground state energy of the final atomic arrangement.The numerical algorithms listed below are commonly employed in ab-initio codes to find the ground state energies based on energy and gradients

- Conjugate-gradient (CG) method.
- Residual minimization method (RMM)
- Quasi-Newton method
- Variable metric method (BFGS)

2.3 Optical Propeties of GaX (X=P, As, Sb)

The study of optical properties of pristine GaX (X= P, As, Sb) has special significance in science, technology and industry for the development of new optical devices. The first-principles calculations of the optical properties pristine of GaX (X= P, As, Sb) mainly include absorption coefficients($\alpha_{abs}(\omega)$), dielectric functions(ε), the reflectivity $R(\omega)$, extinction coefficient$\kappa(\omega)$ and refractive index are simulated by converting the complex dielectric function. At quantum mechanical level in bulk solids the complex dielectric functions is closely connected with the band structure. The real part of the dielectric function can be calculated by

$\varepsilon_1(\omega)$ using the Kramers-Kronig formula is $\chi(\omega) = \chi_1(\omega) + i\chi_2(\omega)$ where i be a complex function of the variable ω, $\chi_1(\omega)$ and $\chi_2(\omega)$ are real parts . The imaginary part of the dielectric function $\varepsilon_2(\omega)$, can be described by the selected regularity momentum matrix elements satisfied by the valance band(occupied) and conduction band (non-occupied) state wave functions. The absorption coefficient can be derived from $\varepsilon_1(\omega)$ and $\varepsilon_2(\omega)$

Dielectric Function

The dielectric function measures the electric displacement field due to the presence of an electric field in a dielectric material.The optical properties are reflected by calculating the complex dielectric function [46, 47]. In the band structure, the transition between the conduction band and the valence band can be explained by the complex dielectric function. The ground state-time-dependent perturbation theory can describe the interaction between the electronic and external fields of the system. Transitions between occupied and non-occupied states, including plasmons and single-particle excitations, are generally caused by the radiation field. The spectrum of these excitations can be represented by the joint density of valence bands and conduction bands. The dielectric function serves as a bridge between the microscopic physical processes and the solid electronic structure of the inter-band transitions, reflecting the information of other spectra. In summary, the correspondence between the real and imaginary parts of the dielectric function can be found by the energy band structure and the density of states. The complex dielectric function [46] is expressed as:

$$\varepsilon = \varepsilon_1(\omega) + i\varepsilon_2(\omega) \tag{2.51}$$

The imaginary part $\varepsilon_2(\omega)$ is calculated from the density matrix of the electronic structure [49]according to the implementations given by

$$\varepsilon_2(\omega) = \frac{8\pi^2 e^2 \hbar^2}{\Omega\omega^2 m_e^2} \Sigma_{k,v,c} w_k |\langle \Psi_k^c | u.r | \Psi_k^v \rangle|^2 \delta(E_k^c - E_k^v - \hbar\omega) \tag{2.52}$$

where e is the electronic charge, and Ψ_k^c and Ψ_k^v are the conduction band (CB) and valence band (VB) wave functions at k, respectively,$\hbar\omega$ is the energy of the incident photon, $u.r$ is the momentum operator,w_k is a joint density of states, and Ω is volume of the primitive cell. The Real part $\varepsilon_1(\omega)$ of the dielectric function can be found from the KramersKronig equation (2.52).

$$\varepsilon_1(\omega) = 1 + \frac{2}{\pi} P \int_0^\infty \frac{\omega' \varepsilon_2(\omega)}{\omega'^2 - \omega^2} d\omega' \tag{2.53}$$

Where, P stands for the principal value of the integral. The optical absorption coefficient was obtained by using Eq.(2.54).

$$\alpha_{abs}(\omega) = \sqrt{2}\frac{\omega}{c}\sqrt{\sqrt{\varepsilon_1^2(\omega) + \varepsilon_2^2(\omega)} - \varepsilon_1(\omega)} \tag{2.54}$$

where ω is photon frequency, and c is speed of light. ε_1 and ε_2 are frequency dependent real and imaginary parts of dielectric function as stated in Eq.(2.52). The

photocurrent density under irradiation with a certain wavelength can be described by an empirical Glass Law[50].

$$J_{ph} = \alpha \kappa I \tag{2.55}$$

where α is the optical absorption coefficient,κ is a material-dependent Glass coefficient, and I is irradiation intensity. The relation between α and an optical band gap E_g^o can be estimated using the concept of Tauc relation as elaborated elsewhere.

$$\alpha(\hbar\omega) \sim A(\hbar\omega - E_g^o)^{\frac{1}{2}} \tag{2.56}$$

where A is a material dependent constant and $\hbar\omega$ is the incident photon energy. The Reflection Coefficient which measures the fractional amplitude of the reflected electromagnetic field is given by:

$$R(\omega) = \frac{n(\omega) - 1 + ik(\omega)}{n(\omega) + 1 + ik(\omega)} \tag{2.57}$$

where n is the refractive index and k is the extinction coefficient.

Absorption Coefficient

One of the most important optical properties as an absorber material in a solar cell is to absorb the sunlight efficiently. The absorption coefficient $\alpha(\omega)$ describes this efficiency in units of $\frac{1}{length}$. That is, if the absorption coefficient is large, the thickness of the absorber material can be thinner while still absorbs the same amount of sunlight. The absorption coefficient is related to the dielectric function through the expression in $Eq.2.54$. The imaginary part $\varepsilon_2(\omega)$ of the dielectric function is closely related to the absorption coefficient; for instance, both $\varepsilon_2(\omega)$ and $\alpha(\omega)$ are zero for photon energies smaller than the band gap. That is, by analyzing the dielectric function one can also understand how the optical transition occurs and how good or bad the material is for a solar cell. The imaginary part of the dielectric function$\varepsilon_2(\omega)$ in atomic units is given by equation(2.52) [48].

$$\varepsilon_2^{ij}(\omega) = \frac{Ve_2\kappa}{2\pi^2\omega^2}\int d^3\kappa \sum_{nn'} \langle \kappa n_i|\kappa n'\rangle\langle \kappa n'|P_j|\kappa n\rangle \times f_{\kappa n}(1 - f_{\kappa n'}\delta(f_{\kappa n'} - f_{\kappa n} - \hbar\omega)$$

$$= 8\pi^2\omega^{-2}\Omega^{-1}\sum_{nn'k} w_k f(\varepsilon_{nk} - f(\varepsilon_{n'k})\sigma(\varepsilon_{n'k} - \varepsilon_{nk} - \omega)\langle\psi_{n'k}|\nabla_\alpha|\psi_{nk}\rangle\langle\psi_{n'k}|\nabla_\beta|\psi_{nk}\rangle$$

. Where $P = (P_x, P_y, P_z)$ is the momentum operator, $f_{\kappa n}$ is Fermi distribution, and κn is the crystal wave function, corresponding to energy $\varepsilon_{\kappa n}$ with momentum κ. Imaginary part of the dielectric function $\varepsilon_2(\omega)$ will be calculated by the DFT. And the real part of the dielectric function $\varepsilon_1(\omega)$ is then calculated using the Kramers-Kronig relation as given by Equation (2.53).

$$\varepsilon_1^{ij} - 1 + \frac{2}{\pi}P\int_0^{\inf} \frac{\varepsilon_2^{ij}(\omega')\omega'}{\omega'^2 - \omega^2 - i\eta}d\omega'. \tag{2.59}$$

These two spectra are then used to calculate all the other optical spectra by DFT

with in GGA-PBE, and LDA+U approximation using the following expression[48]. The absorption coefficient indicates the percentage of attenuation of light intensity per unit of propagation distance of the light wave in the medium. The formula is given by

$$\alpha(\omega) = \frac{4\pi}{\lambda} k(\omega) \tag{2.60}$$

where $k(\omega)$ is the extinction coefficient and λ is the wavelength in nm multiply by 10^7 to get the absorption coefficient in the unit of cm^{-1}. The transmittance is obtained from the relation $R + T + A = 1$ .where R, T and A represent the reflectance, transmittance and absorbance respectively. The sum of these macroscopic quantities must equal unity since the incident radiant flux at one wavelength is distributed totally between reflected, transmitted and absorbed intensity. The extinction coefficient is a characteristic that determines how strongly a species absorbs or reflects radiation or light at a particular wavelength. The extinction coefficient is a characteristic that determines how strongly a species absorbs or reflects radiation or light at a particular wavelength. The exitinction coefficient is given by:

$\kappa_e(\omega) = \frac{\sqrt{\sqrt{\varepsilon_1^2(\omega)+\varepsilon_2^2-\omega_1(\omega)}}}{2}$ (2.61)

$\kappa\omega = \frac{2\pi c}{\lambda}$ (2.62)

where$\kappa(\omega)$ is the frequency, c is the speed of light and λ is the wavelength. $\varepsilon_1(\omega)$ describes how much the material is polarized when an electric field is applied, and $\varepsilon_2(\omega)$ is related with absorption of the material.

Refractive Index

In optics, the refractive index (or refraction index) of an optical medium is a dimensionless number that gives the indication of the light bending ability. Complex refractive index [46] can be expressed as:

$$N(\omega) = n(\omega) + ik(\omega)n(\omega) = \frac{\sqrt{\sqrt{\varepsilon_1^2(\omega) + \varepsilon_2^2(\omega)} - \varepsilon_1(\omega)}}{2} \tag{2.63}$$

where $n(\omega)$ is the refractive index and $\kappa(\omega)$ is the extinction coefficient. The relationship between the real part, the imaginary part and the permittivity of the refractive index. Reflectivity is defined as the reduction in reflected power caused by the introduction of an absorbing material. The Reflectivity is given by

$$R(\omega) = |\frac{\sqrt{\varepsilon(\omega)} - 1}{\sqrt{\varepsilon(\omega)} + 1}|^2 = \frac{(n(\omega) - 1)^2 + k^2(\omega)}{(n(\omega) + 1)^2 + k^2(\omega)}]$$

Photoemission

It is the energy measurement of electrons emitted from solids, gases or liquids by the photoelectric effect, in order to determine the binding energies of electrons in a substance [51]

Suseptibility

Electric susceptibility, χ_ϵ quantitative measure of the extent to which an electric field applied to a dielectric material causes polarization, the sight displacement of positive and negative charge within the material [51]. For most linear dielectric materials, the polarization P is directly proportional to the average electric field strength E so that the ratio of the two, P/E is a constant that expresses an intrinsic property of the material. The electric susceptibilty, χ_ϵ is defined as:

$$\chi_\epsilon = \frac{P}{\epsilon_o E} \tag{2.65}$$

.

2.4 Structural, Electronic, and Optical properties of Graphene

2.4.1 Structural properties of Graphene

Carbon atoms are arranged in a single sheet called graphene. The hexagonal crystal lattice that the carbon atoms are organized in is the result of their sp^2-hybridization. In figure2.4 this structure is depicted schematically. Graphene's atomic structure is comparable to that of chicken wire or a honeycomb. Scanning tunneling microscopy (STM), for instance, was used to confirm this structure,[52]. In graphene, the distance separating two carbon atoms is approximately 0.142 nm. Despite being viewed as a flat sheet, graphene actually has ripples. Theoretical calculations [54] and experimental observation [53] both indicate an out-of-plane displacement of roughly 1nm. These ripples have a lateral size distribution of 50100 nm. The existence of these ripples could be the key to the stability of relatively large graphene sheets are stable at all. They could be viewed as a device to lessen thermal vibrations. They can be seen as a mechanism to lower the thermal vibrations that threaten the stability of all two- dimensional layers. Graphene can be considered as the base material from which other sp^2 carbon allotropes can be folded. The interlayer spacing in stacks of multiple layers is 0.335nm. The layers in few-layer graphene (FLG) and graphite are held together by weak van der Waals forces.

2.4.2 Electronic properties of graphene

The electronic properties of graphene have opened new doors in physics and they are often described as exotic and unique. Charge carriers in graphene cannot be described with regular nonrelativistic quantum mechanics and the Schrdinger

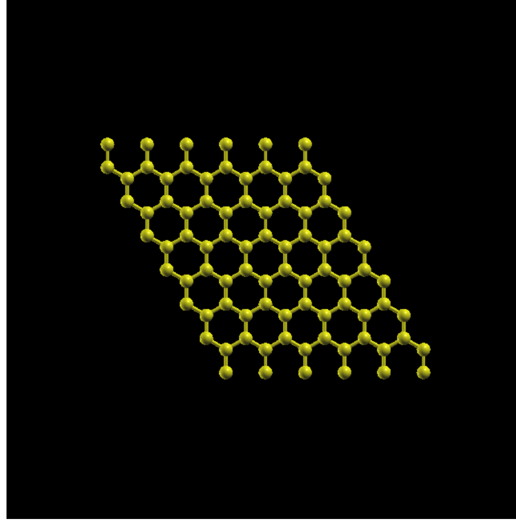

Figure 2.4: structural properties of graphene

equation. They obey the rules of relativistic quantum mechanics also called quantum electrodynamics (QED). Charge carriers in graphene are described as massless Dirac fermions. This type of physics could be observed only in cosmology and high-energy particle accelerators. With the discovery of graphene however,these phenomena of quantum electrodynamics can be studied in the laboratory. For now,graphene is the only solid known to exhibit these quantum electrodynamics [55]. This is partly due to the fact that graphene can be produced or isolated with exceptional crystalline quality. Other existing 2D materials lack this electronic quality. A single graphene layer is a zero-gap semiconductor. The electronic band structure of graphene is determined by its orbitals. The valence and conduction bands touch each other at the K points,also called Dirac points. These K points are the corners of a two-dimensional hexagonal Brillouin zone. There are actually three K points and three K points linked to the two sublattices of graphene. The low energy band structure around these K points resembles two touching cones with a linear energy-momentum (E-k) dispersion relation. The dispersion relation is given by the following equation:

$$E = |\hbar.k|\nu_f \tag{2.66}$$

where $\hbar.k$ is momentum and ν_f is the Fermi velocity. The Fermi velocity in this case is $10^6 ms^{-1}$, which is 300 times slower than the speed of light. A consequence of this linear dispersion relation is that the charge carriers be have as massless particles[56, 57, 58].

2.5 Absroption Energy of GaX (X=P, As, Sb) on graphene

The most favorable adsorptions have adsorption energies in the range [-58.47,-17.07, 8.15]eV for a carbon adsorbate at 1 ML adsorbate coverage. With the adsorption of graphene, these values are in the range of [22.16,34.76, 48.63]eV.

The relatively lower adsorption energies of carbon compared to graphene could indicate that the respective ions have better mobility within the electrolyte. Furthermore, GaSb is a more favorable as well as reactive surface with the adsorbates at higher fuel supplies, thus, it better represents a typical surface of GaAs alloy. A charge of about 0.261e per carbon atom appears to be released to the system for electricity contribution. Finally, the importance of graphenes superior conductivity is not impacted by its interaction with GaX,according to the fact that its Dirac point is unaffected despite its adsorption on GaX. In hybrid systems,excited electrons with energies between 0 and 3 eV (against Fermi energy) are primarily accumulated on graphene. The calculations offer a theoretical justification for the successful operation of graphene/GaX hybrid materials as photocatalysts and solar cells

2.5.1 Spin polarization

An essential characteristic of electron-electron interactions in electronic systems is spin polarization. An open-shell atom has unpaired electrons in its ground state, which allows it to carry a magnetic moment via spin polarization in valence orbitals. According to a nave theory, in order to maximize the decrease of the electron-election repulsion by making use of the Pauli exclusion principle, the magnetic moments would be aligned in parallel among neighboring atoms
However, the double electron occupancy of bonding (delocalized) orbitals is favored by energy reduction through the creation of chemical bonds or electron delocalization, which results in an antiparallel spin alignment or even a spin unpolarized electronic structure. No one of two conflicting effects is consistently dominant in molecules and solids, according to observations of different magnetic behaviors. Understanding the competition and its effects, particularly in solid-state molecules, is difficult on two different levels. First, multiple magnetic compounds exist, and understanding their properties seems to require distinct conceptual foundations for each one. Second, various models for various forms of magnetism have been constructed with varying degrees of approximations and sophistications. A unified conceptual model known as "spin polarization perturbational orbital theory (SPPOT)" is presented in this chapter as an analysis of the conventional models[59].

Chapter 3

Methodology

3.1 Implementation of Density functional theory(DFT)

All calculations in this work were carried out using the gradient projected augument wave (GPAW)code,which was implemented in the ab initio simulation and cited in [60]. The exchange-correlation energy of the interacting electrons is expressed using the frozen-core full potential projector augmented wave (PAW) approach [61] and the Perdew-Burke-Ernzerhof (PBE) form [62].The electronic ground state was determined using the plane waves basis with a cut-off energy of 400eV and the conjugate gradient algorithm,with the convergence threshold set at 5×10^{-4} eV for energy and 0.05 eV for force. The Brillouin zone integrations were carried out using Monkhorst-Pack grids,citing by [63]
We used k-point meshes of $6 \times 6 \times 6$ for a zinc blende GaX primitive cell,$6 \times 6 \times 6$ for a graphene primitive cell and GaX ($1\times$) polar surfaces and $6 \times 6 \times 6$ for the supercells of the interface. A dipole correction [64] was applied to make the computation converge more quickly and eliminate the artificial electrostatic field between periodic supercells.

3.1.1 Hubbard U scheme (DFT+U)

Since DFT−GGA severely underestimates the band gap of GaX by giving a wrong energy position of the Ga 3d orbital,we adopted the GGA + U method of Dudarev et als approach [65]] to partially correct this issue,where the effective on-site Coulomb interaction parameter U and exchange interaction parameter J are 6.5 and 1.0 eV, respectively. Although adopting hybrid functionals,where the Hartree-Fock exchange is partially combined with the DFT exchange, would be a more accurate strategy,it would be prohibitively expensive from a computing standpoint because this material has too many orbitals for Hartree-Fock to handle. Traditional density functionals are unable to give a correct description of van der Waals (vdW) interactions because of dynamical correlations between fluctuating charge distributions.In the models of the interface,vdW interactions are expected to be dominant and thus the DFT-D2 method of Grimme [66],which is successful for graphene/SiC interface structures [67] was adopted in this work.The total energy (E_{total}) is represented as:

$$E_{total} = E_{KS-DFT} + E_{vdW} \tag{3.1}$$

where E_{KS-DFT} is the conventional Kohn-Sham DFT energy and E_{vdW} is the dispersion correction [68] for details). Note that Vanin et al[69]reported that the vdW-DF method proposed by Dion et al [70] failed to reproduce the experimental observations of the metal-graphene interface
Density functional theory(DFT)is a computational quantum mechanical modeling method used in physics, chemistry and materials science to investigate the electronic structure,optical novel properties of pristine and carbon supported GaX (X=P, As, Sb) many-body systems,in particular atoms, molecules, and the condensed phases. The fundamental principle of density functional theory(DFT) is that any property of the system of many interacting particles can be viewed as a functional of the ground state density ($n_o(r)$); that is one scalar function of position, in principle determines all the information. In this thesis the calculations were performed using Atomic Simulation Enviroment(ASE) using simulation with GPAW package software within framework of DFT and plane wave pseudo potential method. In Khon Sham equations, the exchange correlation potential is difficult to predict and a puzzling term in DFT. To approximate this potential,LDA ,PBE, GGA+U,and hybrid (PBE0) functionals are adopted. The interaction between core and valance electrons was treated using Projector augmented-wave pseudo-potential (PAW) in LDA, PBE and DFT+U approximations and norm-conserving pseudo-potential in PBE0 approximation. While approximating this potential the core electrons which cannot participate in the chemical bonding of the system are frozen and only valence electrons are considered. The number of valence considered for each elements within the PAW data set is Ga:31, P:15,As:33 and Sb:51. Therefore,the electron configuration of $Gallium(Ga^{31})$ is $[Ar]4s^2 3d^{10} 4p^1$,$Phosphrous(P^{15})$ is $[Ne]3s^2 3p^3$, $Arsnide(As^{33})$ is $[Ar]3d^{10} 4s^2 4p^3$ and $Antimonide(Sb^{51})$ is $[Kr]4d^{10} 5s^2 5p^3$
In this calculation the experimental values of lattice parameter of the GaX was used. For convergence tests, Pseudopotential, the electronic wave functions are expanded in a plane-wave basis set with trial cutoff energy. The k-point sampling of the Brillouin zone(BZ) was constructed using Monkhorst-Pack mesh scheme. Convergence test of total energy with respect to energy cutoff and k-point sampling performed to ensure the accuracy of the calculations until the change in energy is equal to 0.05 eV. After convergence test was made, we performed a one-shot calculation to obtain the value of u for Ga in each compounds

3.1.2 GPAW code

GPAW is a density-functional theory (DFT) Python code based on the projector-augmented wave (PAW) method and the atomic simulation environment (ASE).The wave functions can be described with:
- Plane-waves (pw)
- Real-space uniform grids, multigrid methods and the finite-difference approximation(fd)
- Atom-centered basis-functions (lcao)

3.1.3 Technical Detail Convergence test

Plane Wave Basis Sets

Any appropriate basis set can be utilized to enlarge the electron orbitals that are used to represent the single particle states. The Bloch theorem-based plane wave basis set is employed in practice with the advantages listed below. Due to the Bloch theorem, plane waves are the obvious choice for the representation of electron orbitals in a periodic system, and the kinetic energy operator is diagonal in a plane wave representation. A plane wave basis set is impartial and does not assume any preconceptions on the form of the problem. The k-points and cut-off energies selected would have an effect on the overall energy of the systems since the plane wave basis set is employed for the expansion of electron wave functions. The Hamiltonian of the Kohn-Sham equations in the unit cell expands the unknown electronic orbitals Ψ_{nk} in a full set of periodic known basis functions. One possibility for the wave functions is the planar Bloch wave function. According to Blochs theoram, an electron in a priodic potential has a wave function can be written as:

$$\Psi_{nk}(r) = e^{ikr}u_{nk}(r) \tag{3.2}$$

. Where Ψ is a wave function at an arbitrary wave vector. Where u_{nk} is a space-dependent amplidude function which reflects the periodicity of the lattice $u_{nk}(r) = u_k(r + R)$ for R is lattice vector,k is wave vector of the particle can be choosen within the frist Brillouin zone,r is its position. Since u is a periodic function it can be expanded using a discrete set of sum over reciprocal lattice vectors G.

$$u_{nk}(r) = \sum C_{n,k} + G^e iG.r \tag{3.3}$$

Thus the electronic wave functions can be written as:

$$\Psi_{nk}(r) = \sum_G C_{n,k} + G^e i(k + G).r \tag{3.4}$$

The electronic wavefunctions at each k-point expressed in terms of a discrete plane wave basis set.

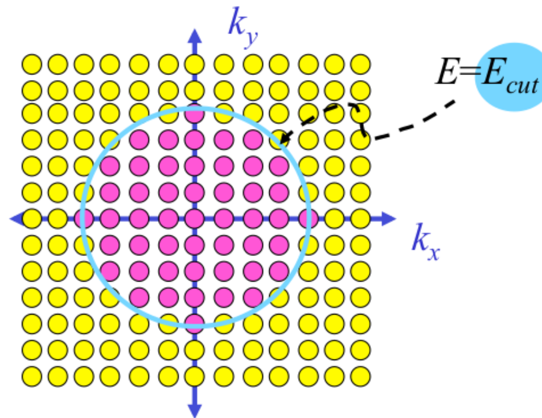

Figure 3.1: Truncating the plane wave expansion.

All-electron wavefunctions have nodes close to the atomic nucleus, which require a large number of basis functions to describe. By stating that all-electron and pseudo-wavefunctions should be the same beyond a certain radial cut-off the wavefunctions of the valence electrons are preserved; while the wavefunctions close to the atomic core can be made smooth, and node-less. The plane wave cutoff energy is given by:

$$E_{cut} = \frac{G_{cut}^2 \hbar^2}{2m_e} \tag{3.5}$$

. where; E_{cut} is plane wave cutoff energy, G_{cut} is cutoff at some vector i.e G is vector proportional to the inverse lattice vectors of the supper cell and m_e is mass of electron. The core electrons usually do not significantly contribute to the bonding. In principle this Fourier series is infinite. However, in practice we cannot work with an infinite basis set, it has to be truncated. The number of plane waves can be restricted by placing an upper boundary to the kinetic energy of the plane waves. This boundary is called energy cut-off E_{cut} and only plane-waves satisfying the condition, $\frac{|k+G|}{2} < E_{cut}$ are considered in the computation. With DFT the complexity of the problem has reduced appreciably. However, for systems with a large number of electrons, it still remains computationally very expensive

K-point sampling(Convergence)

It was discussed how Blochs theorem allows one to only consider the electrons within the unit cell at an infinite number of k-points within the first Brillouin zone. It is possible to use only a finite number of k-points if these are chosen so as to appropriately sample the reciprocal space. One can therefore write an integrated function f(r) over the Brillouin zone as:

$$f(r) = \frac{\Omega}{(2\pi)^3} \int_{BZ} F(r)dr = \sum_j \omega_j F(r_j) \tag{3.6}$$

. where $F(r)$ is the Fourier transform of$f(r)$, Ω is the cell volume, $\frac{\Omega}{(2\pi)^3}$ is their density and the ω_j are weighting factors. The electronic density in DFT is calculated through the integration of the square modulus of the Bloch functions on all occupied energy bands and over the Brillouin zone [63].

$$n(r) = \sum_\alpha \int |\Psi_{nk}(r)|^2 f_{\alpha k} dk \tag{3.7}$$

. Where $f_{\alpha k}$ is the occupation of the state k in the band α and $\Psi_{nk}(r)$ is the corresponding Bloch wave function. The integration over the reciprocal space involves the choice of an optimal finite set of k-points, which is often referred to as Brillouin zone sampling. Monkhorst and Pack proposed unbiased methods of choosing a set of k-points for sampling the Brilloun zone. According to Born-von Karman periodic boundary conditions, in fractional coordinate, it is a rectangular grid of points of dimensions$N = N_1N_2N_3$ equally spaced mesh throughout the Brillouin zone where N_1, N_2, and N_3 are positive integers. N_i is the number of unit cells in the ith direction, for $i = 1, 2, 3$, and G_i are its primitive lattice vectors. The method proposed by Monkhorst-Pack, is one of the most widely used sampling

techniques, which allows to sample a uniform grid of k-points along each direction, using a simple formula:

$$k_{m_1,m_2,m_3} = \sum_{i}^{3} \frac{m_i}{N_i} G_i \tag{3.8}$$

. Where the m_i are integers, Each time that all of the m_i change by one we generate a new state; therefore the volume of k-space occupied by one state is $\frac{A_1}{N_1} \cdot \frac{A_2}{N_2} \times \frac{A_3}{N_3} = \frac{1}{N} A_1 . A_2 \times A_3$ where N_i is the discretization number in the direction of the reciprocal lattice vector G_i . Thus,the total number of k-points is N. The larger the dimensions of the grid the finer and more accurate will be the sampling. The number can be decreased by considering the symmetry of the system, which can effectively speed up the calculation. It is worth noting that the number of k-points which is required to give a good estimate of the system depends on all aspects of the system such as size and structure. Thus, it is necessary to check if the k-point grid can give converged results. One also has to be careful when the energies of the unit cell are compared in different sizes, unless either equivalent k-points are used or the total energy is found to be conserved.

Pseudopotential

It is well known that valence electrons have the dominant role in determining the majority of physical properties of solids, as opposed to the core electrons that are strongly bound to the nucleus and almost insensitive to the chemical environment. This motivates the idea that one can, in one way or another, keep only the valence electrons in practical DFT calculations, and merge the core electrons with the nucleus by using an effective pseudopotential. Pseudopotentials helped in a crucial way to make the calculations tractable. Using the fact that the physical properties of solids depend mainly on valence electrons, the computational effort can be minimized considerably. In the pseudopotential approximation, the core electrons are removed and the strong ionic potential is replaced by the weaker pseudopotential (V_{pseudo}) that acts on a set of pseudo wave functions(Ψ_{pseudo}) rather than the true valence wave functions(Ψ_{AE}).

.

The pseudopotential approximation is to replace the complicated effects of the core electrons of an atom and its nucleus so that the Schrodinger equation contain the modified effective potential term instead of coulomb potential for the core electrons. Because the outer shell of electrons that contribute to the majority of the physical properties of the element. The core electrons, do not play a significant role in the bonding properties of the element. The pseudopotential replaces the all-electron potential with one that simulates only the chemically active valence electrons states. For the chemical properties of the element to behave properly the pseudopotential must still match the original all-electron potentials properties. Within the atomic core the pseudopotential replaces the core electrons with a potential that is weaker at the core but beyond the distance from the center(r_c), in the chemically active region, the pseudo-wave functions behave like the all-electron wave functions. It can be seen from Figure 3.2 the real and the pseudo wavefunction and potentials match above a certain cutoff radius r_c

The three types of Pseudopotentials used were: ultrasoft pseudopotential, Norm

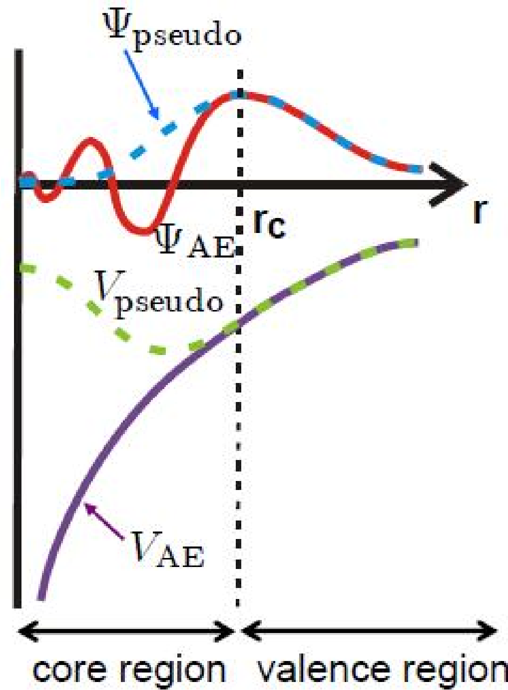

Figure 3.2: Approximations of Pseudopotentials

conserving pseudopotential and Projector-augmented wave (PAWs) pseudopotential.

Norm-conserving Pseudopotential

Norm-conserving pseudopotential allow a basis-set with a significantly lower cut-off to be used to describe the electron wavefunctions and so allow proper numerical convergence with reasonable computing resources.The term norm-conserving simply implies that the pseudopotential possesses exactly the same atomic charge density and inside and outside the cutoff radiusr_c , the norm of each pseudo wavefunction must be identical to the its corresponding all-electron potential(Jonathan,1997) wavefunction

Ultrasoft Pseudopotentials

An ultrasoft pseudopotential was developed by Vanderbilt (1990) to achieve a reduced basis set size by introducing a generalized eigenvalue problem with a non-zero difference in norms we can now defined:

Projector-augmented wave (PAWs) pseudopotential

The projector augmented wave method (PAW) is a technique used in ab-initio electronic structure calculations. It is a generalization of the pseudopotential and linear augmented-plane-wave methods, and allows for density functional theory calculations to be performed with greater computational efficiency (Blochl,

1994; Holzwarth et al, 1996). It is exact when converged (no transferability problems),accuracy is comparable to all-electron techniques (Kresse and Joubert, 1998). PAW is most transferrable, even for atoms that are difficult for Ultrasoft Pseudopotentials. The PAW method is typically combined with the frozen core approximation, in which the core states are assumed to be unaffected by the ions environment

3.1.4 Spin polarization

An essential characteristic of electron-electron interactions in electronic systems is spin polarization. An open-shell atom has unpaired electrons in its ground state, which allows it to carry a magnetic moment via spin polarization in valence orbitals. According to a nave theory, in order to maximize the decrease of the electron-election repulsion by making use of the Pauli exclusion principle, the magnetic moments would be aligned in parallel among neighboring atoms. However, the double electron occupancy of bonding (delocalized) orbitals is favored by energy reduction through the creation of chemical bonds or electron delocalization, which results in an antiparallel spin alignment or even a spin un-polarized electronic structure. A unified conceptual model known as spin polarization perturbational orbital theory (SPPOT) is presented in this chapter as an analysis of the conventional models[59]. Spin polarized calculation is applied where a magnetic moment on each atom is allowed to relax to optimum value. The ZB structures within is considered in this work where the unit cells contain 8 atoms for each GaX(X=P,As,Sb)compounds. Upon setting-up of these structures, literature resources have been closely monitored. Density of states (DOS) is calculated as a population of states available for occupation at a given energy. Brillouin zone integration were performed with the tetrahedron method which is proved efficient especially for excited states and magnetically induced dielectric function calculation. Ground state calculation is performed with k-point density of 5 points per with -point inclusion. A restarted calculations were done with a fixed density of 6.0 points per over densely sampled k-points grid. The k-point density is calculated as:

$$N\frac{a*}{2\pi} \tag{3.9}$$

where N is the number of k-points and is the reciprocal of a lattice vector of the unit cell. Spin polarized treatment is applied to the calculations. Equilibrium volumes and bulk modulus are calculated using Murnaghan equation of state. Cohesive energy is calculated as the energy required to break atoms of the solid into a constituent isolated atoms, as described elsewhere.

Chapter 4

Results and Discussion

4.1 Result of DFT

4.1.1 Bulk Properties of GaX

Equation of state (EOS)

Employing the equation of state for several compounds, we were able to determine the equilibrium lattice constant and the material's resistance to external pressure(Bulk modulus), using the equation of state (EOS) for bulk GaX(X=P,As,Sb) structures before we proceed to the results obtained in graphene/GaX(X=P,As,Sb) hetrostructures. A semiconductor group III−IV material with bulk modulus structures is gallium X (GaP, GaAs, and GaSb)[70, 71] . The energy-versus-volume calculation method used to derive the EOS also outputs a number of other significant bulk structural characteristics, such as minimum volume and minimum energy.

Equilibrium lattice constant, Bulk modulus, Cohesive energy and Formation energy

The lattice constant, which we have determined, can be extended and used to estimate the volume and density of a crystal, making it possible to establish the structural information of a material more quickly. This is crucial when creating new materials since the process of creating new materials frequently calls for certain structural requirements. The bulk modulus, which assesses a material's capacity to with stand changes in volume under uniform compression or expansion, is the most basic isothermal EOS for a solid.

Cohesive energy bulk of GaX (X=P, As, Sb)

When analyzing phase stability, the cohesive energy, or($E_{coh} eV/atom$), is used to describe the strength of the forces holding atoms together in the solid state. The energy needed to separate a solid's atoms into discrete atomic species is known as the cohesive energy of the solid. A number of significant characteristics can be predicted by employing cohesive energy, which is one of the metrics used to understand the nature of chemical bonding. Its size provides information on stability and chemical reactivity. Since different alternative structures would have

different cohesive energies, in the end, the quantity decides the structure [72, 73]. It is calculated by:

$$E_{coh} = \frac{1}{N} | \sum E_{atom} - E_{bulk} | = \frac{NE^{Ga}_{atom} - NE^{X}_{atom} - E^{GaX}_{Tot}}{N_{Ga} + N_X} \quad (4.1)$$

Where N is the number of atoms in the unit cell of the gallium X compound atoms and E_{coh} is the cohesive energy. The atomic energy of a gallium X(X=P, As, Sb) atom in its ground state is E_{atom}. As a result, the estimated cohesive energies for GaAs, GaSb, and GaP are $3.74eV/atom$, $3.24eV/atom$, and $1.42eV/atom$, respectively, as also shown in table 4.1. We are implying that based on the computed values of cohesive energy, GaAs > GaSb > GaP. When we compared the cohesive energy values of the three materials, GaAs, GaSb, and GaP, they were found to be 3.74eV/atom,> 3.24eV/atom,> 1.42eV/atom, respectively. Since GaAs has a higher value, this suggests that it is more stable than the other two materials.

Formation Energy bulk of GaX (X=P, As, Sb)

Formation Energy(E_f) is the energy required to dissociate the materials into individual components. The energy necessary to form the alloy compound from its separate elemental bulk structures is represented by energy formation, $E_f(eV/atom)$, which is given by

$$E_f = \frac{1}{N} E_{bulk} - \sum_i \frac{1}{N_i} E^i_b E_f = \frac{E^{GaX}_{Tot} - NE^{Ga}_{solid} - NE^{X}_{solid}}{N_{Ga} + N_X} \quad (4.2)$$

. Where N_{Ga} and N_X is number of atoms in the Ga and X bulk unit cell of the alloy of gallium X compound, E_{bulk} is total energy of the bulk alloy gallium X compound, E^i_b is total energy of bulk of element i, and N_i is number of atoms in the unit cell of the elemental bulk form. GaX(GaP, GaAs, and GaSb) are assumed to have a face-center cubic structure throughout calculation (FCC). For GaAs, GaP, and GaSb, respectively, the calculated formation energies(E_f) values are -0.81eV, -0.57eV, and -0.56eV. GaAs< GaP< GaSb have formation energies (E_f) of -0.81eV <-0.57eV<-0.56eV respectively (see table 4.1). All of the minimum energies, shown in table (4.1), are negative. Such low values of(E_f) imply that the GaX(X= P, As, Sb) phases are thermodynamically advantageously created, and this stable structure is most likely to exist throughout this investigation. Additionally, the bulk modulus(B) values for GaP > GaAs > GaSb are 77.3GPa> 52.4GPa> 46.0GPa, respectively. GaP has a relatively better working and endurance capacity under pressure, according to GaSb. The author has complete faith in the validity of the model employed in this work because the optimal geometric structural properties shown in table (4.1) compare rather favorably with experiments. It seems vital to examine the possibility of significant vacancy forms as well. It appears also necessary to analyze prospect of bulk vacancy formations. The vacancy formation energy $E_{Vac}(eV)$ is defined as:

$$E_{Vac} = E_\nu - \frac{N-1}{N} E_{bulk} \quad (4.3)$$

E_{bulk} is the energy of an N-atom bulk cell without any vacancy and the E_ν is the bulk potential energy of the same unit cell with a vacancy in it. The vacancy

formation energy is the amount of cohesive energy required to create a vacancy. If this value is negative, it significanes that when a vacancy is formed, energy is released. The comparison of the calculated values of lattice constant, bulk modulus, equilibrium unit cell volume, formation energy and cohesive energy with experimental results are shown in table (4.1)

Table 4.1: Computed the lattice constant $a(\ \mathring{A})$, the bulk modulus $B(GPa)$, formation energy $E_f(eV/atom)$, and the cohesive energies $E_{coh}(eV/atom)$ of selected GaX or GaP,GaAs and GaSb materials systems of this work

		Materials						
Quantity	Source	Ga	P	As	Sb	GaP	GaAs	GaSb
a(Å)	This work					5.54	5.76	6.21
	Experimental	4.52	11.45	3.75	4.31	5.45[a]	5.65[a]	6.10[a]
B(GPa)	This Work	-	-	-	-	77.3	52.43	46
	Experimental	-	11	22	42	88[b]	75.5[b]	56.3[b]
E_f	This Work	-	-	-	-	-0.57eV	-0.81eV	-0.56eV
	Experimental	-	-	-	-	-	-	-
E_{coh}	This Work	-	-	-	-	1.43eV	3.74eV	3.24eV
	Experimental	-	-	-	-	6.75eV[c]	-	-

Reference [a=b,c] implies that[77, 78]. The quality of the fits can be seen in Figure (4.1). Accordingly, the output parameters of lattice constants (a) and bulk modulus (B) for B_3structure in this work are 5.54$\mathring{A}$, 5.76$\mathring{A}$, and 6.21$\mathring{A}$, and 77.3GPa,56.4GPa, and 46GPa respectively. But the experimental results of lattice constants (a) and bulk modulus (B) are 5.45$\mathring{A}[a]$,5.65$\mathring{A}[a]$,and 6.10$\mathring{A}[a]$ and 88$GPa[b]$,75.5$GPa[b]$,56.3$GPa[b]$ respectively. The results presented in table (4.1) show that even if there is small difference in between the computational and the experimental results, the two are essentially in agreement with each other. The experimental results are taken from literatures [74, 75, 76, 77]. Moreover, the graph of lattice constant versus total energy for GaX displayed in Figure below

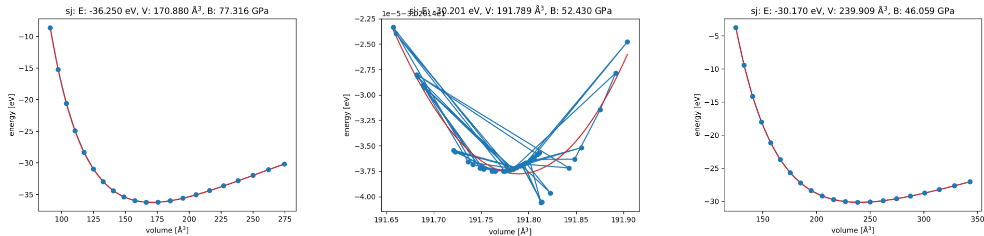

(a) Total energy versus Lattice constant of GaP (b) Total energy versus Lattice constant of GaAs (c) Total energy versus Lattice constant of GaSb

Figure 4.1: Total energy versus Lattice constant of GaX

Convergence Tests

We consider the plane wave basis set is used for the expansion of electron wave-functions(see Equn.(3.3)-(3.4)), the k-points and cut-off energies chosen would impact on total energy of the systems. The K-point convergence of cubic GaX was analysed in the unit cell by varying the Monkhorst-Pack (MP) grid between $2 \times 2 \times 2$ to $12 \times 12 \times 12$ increasing in increments of $6 \times 6 \times 6$. The convergence of the total energy to six significant figure as a function. Our calculations show that k-mesh of$2 \times 2 \times 2$ to $12 \times 12 \times 12$ can be optimum in the bulk calculations these structures, as shown in figure (4.2). With surface calculations, correspondingly, a k-mesh of $6 \times 6 \times 6$ is used With a fixed k-mesh of convrgence at this points

Table 4.2: Total energy convergence of cubic GaX as a function of K-point MP-grid

K-ponts(MP grid size)	2×2 × 2	4×4 × 4	6×6 × 6	8×8 × 8	10×10 × 10	12×12 × 12
Computed Etot(Ry)	-39.410	-36.139	-36.146	-36.147	-36.147	-36.147

A convergence test of the total energy with respect to energy cutoff is shown in figure 4.2

.

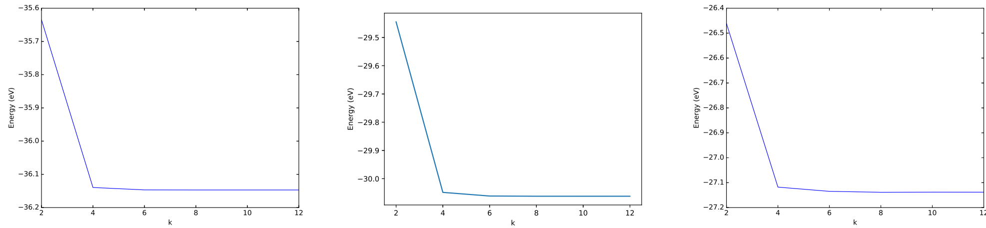

(a) Convergence test of the total energy versus to k-point sampling of GaP (b) Convergence test of the total energy versus to k-point sampling of GaAs (c) Convergence test of the total energy versus to k-point sampling of GaSb

Figure 4.2: Convergence test of the total energy versus to k-point sampling of GaX

Kinetic energy, cut-off (Ecut) convergence

We choose a cut-off energy (ecut) of $400eV$ as an optimum in the rest of our calculations. The kinetic energy cut off convergence is checked by changing the cut off energy. To take both Ecut wfc and Ecut rho in SCF calculations, Ecut and wfc is used since suggested value. Finally total energy against kinetic energy cut-off is shown in figure below. .

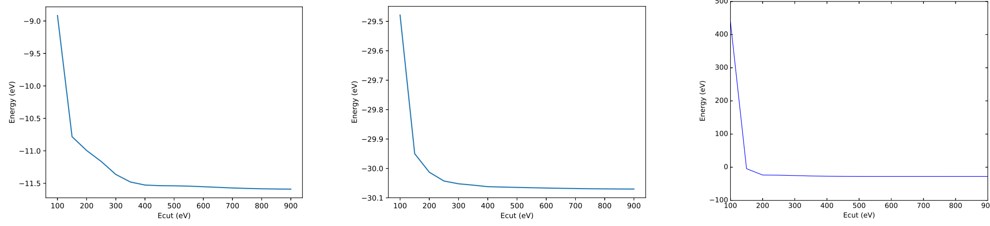

(a) Convergence test of the total energy versus to ecut sampling of GaP

(b) Convergence test of the total energy versus to ecut sampling of GaAs

(c) Convergence test of the total energy versus to ecut sampling of GaSb

Figure 4.3: Convergence test of the total energy versus to ecut sampling of GaX

4.1.2 Electronic Properties of GaX

Band Structures and Bulk Modulus

Band Structures and band gap of Zinc-Blende structure of GaX

When a material has band gaps, a band structure plot can rapidly determine whether they are direct or indirect, how large they are, and if they are metallic, semiconductor, or insulating. Figure (4.4) depicts the band structures of zinc-blende(ZB) GaX(X= P,As,Sb) at room temperature(0K). The bandgap is typically defined as the difference between the eigenvalues of the conduction band minimum (CBM) and the valence band maximum (VBM), which are the bands located at just the first two points on either side of zero (E_f) in the Kohn-Sham description of the system. Band diagrams are helpful in comparing the general band structure characteristics of several materials when they come into touch with one another. The electronic band-gap and band structures plot along high symmetry points of the Birllouin zone of GaX (X = P, As, and Sb) in zinc Blende(ZB) structure are performed within GGA, and Hubbered potential approximations are used to understand how band structure changes relative to the Fermi level in real space. The calculated values of the direct band gaps for GaP, GaAs, and GaSb are $2.29eV$, $1.34eV$, and $0.92eV$, respectively. The band gaps are shown in table (4.3) from the GGA to PBE calculation. It is fairly consistent with the results of the experiment. However, when compared to the experimental values, the values are $2.41eV$, $1.42eV$, and $0.73eV$. The calculated indirect band gaps for GaP, GaAs, and GaSb are $2.29eV$, $1.20eV$, and $0.60eV$, respectively, according to the GGA-PBE calculation. It is fairly consistent with the results of the experiment. However, when compared to the experimental values, the values are $2.26eV$, $1.42eV$, and $0.67eV$. The band gaps calculated by GGA are greater than the equivalent experimental values, which is our conclusion and is evident in table (4.3). The main cause of this underestimating of the band gap is the inability of the simple versions of GGA to adequately recreate the exchange correlation energy and its charge derivative. Whereas our results, which were derived using the GGA approach, showed a high agreement between the experimental data and a reduction in the energy gap. GaAs and GaSb exhibit an overall reduction of the gap over the entire Brillouin zone

Table 4.3: Computed the band gap of the calculated and experimental values of GaX(GaP,GaAs,GaSb) materials systems of this work

			Types of band gap(eV)		
Materials	aÅ)	Sources	Direct	Indirect	Calculated bandgap(eV)
GaP	5.45	This Work	2.29	2.289	
		Experimental	2.41	2.26	1.59
GaAs	5.65	This Work	1.34	2.289	
		Experimental	1.42	1.20	1.019
GaSb	6.10	This Work	0.922	0.60	
		Experimental	0.73	0.67	0.659

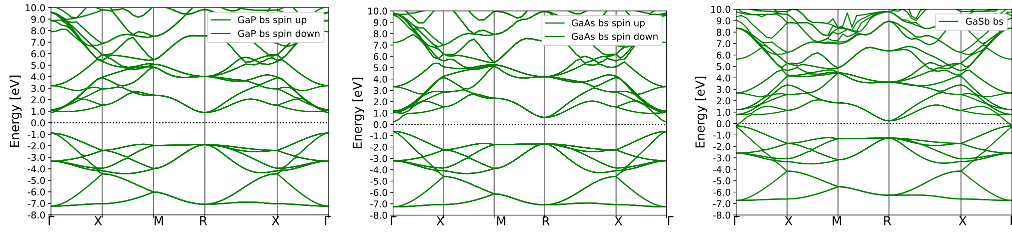

(a) Band Structure of zinc-blende(ZB) for GaP (b) Band Structure of zinc-blende(ZB) for GaAs (c) Band Structure of zinc-blende(ZB) for GaSb

Figure 4.4: Band structure of zinc-blende GaX (X = P, As and Sb) from GGA calculation at 0 K

Density of State (DOS)

Figure (4.5) depicts the zinc-blende GaX (X =P, As Sb) density of states (DOS) and partial density of states (PDOS) at zero kelvin (0K).The density of states (DOS) in solid-state physics displays the number of states per interval of energy as a function of energy, whereas the projection of the DOS onto various angular momentum components (PDOS) is displayed. More particularly, the interaction between various atomic orbitals and the contribution of particular atomic orbitals to the electronic bands are revealed by the PDOS. Figures (4.5- 4.6) describe the DOS and PDOS curves that were described in Section 2.2.1 and in equations (2.48) and (2.49), respectively. The valence band states' density of state (DOS) peaks, which are particularly prominent in the energy $E - E_F$ is [-5, 0]eV. The conduction (occupation) band state of PDOS is influenced by the s, p, and d orbitals, which are depicted in figure (4.5). The occupations with the most states are the p-orbitals, followed by the s-orbitals, which are then followed by the s-orbitals. The s states participate in the deeper energy levels, while the d state has little effect on the energy levels because it is located on the energy level, where the p states dominate the state close to the Fermi level

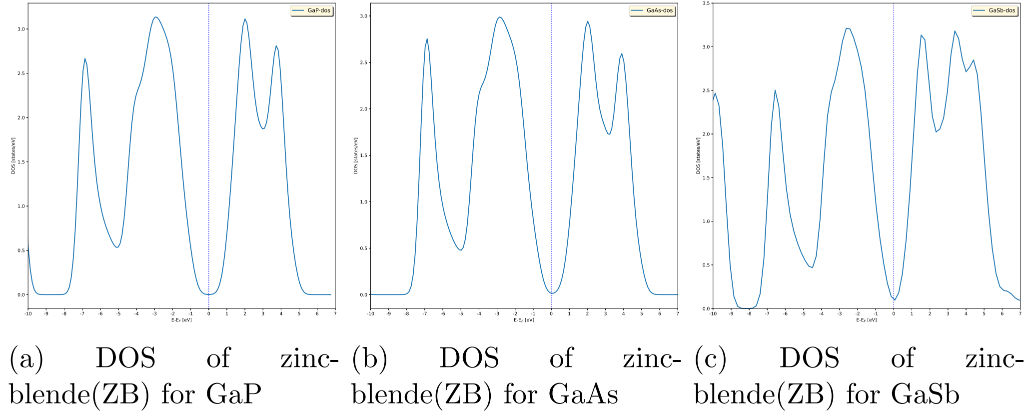

(a) DOS of zinc-blende(ZB) for GaP (b) DOS of zinc-blende(ZB) for GaAs (c) DOS of zinc-blende(ZB) for GaSb

Figure 4.5: Density of States for GaP, GaAs and GaSb

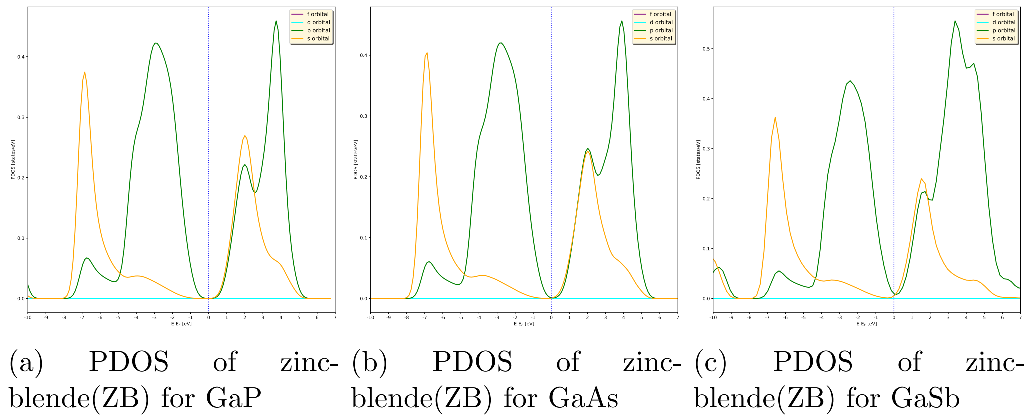

(a) PDOS of zinc-blende(ZB) for GaP (b) PDOS of zinc-blende(ZB) for GaAs (c) PDOS of zinc-blende(ZB) for GaSb

Figure 4.6: Partial Density of States for GaP, GaAs and GaSb

4.1.3 Optical Properties of zinc-blende (ZB) GaX (X=P, As, Sb)

Dielectric constant,Absorption coefficient,Referactive index,Reflectivety

Understanding the optoelectronic applications of GaX (X = P, As, and Sb) requires a thorough analysis of its optical characteristics. The optical characteristics of a medium can be determined from its intricate dielectric function. These characteristics include the dielectric constant, extinction coefficient, refractive index, and absorption coefficient. Combining the real and imaginary components of the permittivity, or $\varepsilon(\omega) = \varepsilon_1(\omega) + i\varepsilon_2(\omega)$, results in a complex dielectric function. The total of all feasible direct transitions from the occupied to unoccupied states over the Brillouin zone is used to determine the imaginary portion of the dielectric function $\varepsilon_2(\omega)$. Equation 2.52, 2.55, and 2.57 were being used, respectively, to compute the absorption coefficient, energy loss function spectrum, and refractive index for the zinc-blende GaX structure. The Bethe Sternheimer equation (bse) and random phase approximation (rpa) data are used to compute the frequency-dependent real $\varepsilon_1(\omega)$ and imaginary $\varepsilon_2(\omega)$ parts of the dielectric function for GaP, GaAs, and GaSb in zinc-blende phase, as shown in Figures (4.7), (4.8), and (4.9), respectively. In the spectra of the real and imaginary sections of the dielectric constant of GaX, there were several peaks corresponding to various electronic

transitions

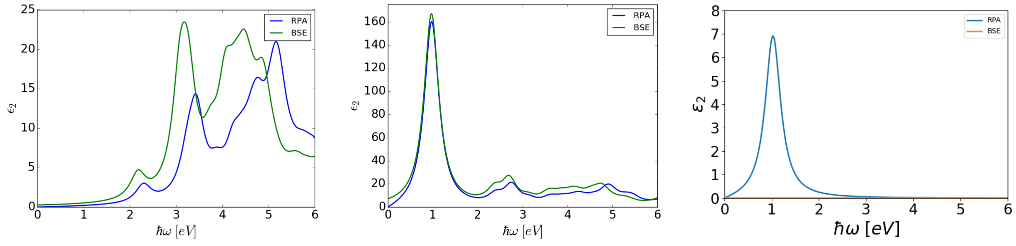

(a) BSE Real and imaginary parts of dielectric constant for ZB of GaP

(b) BSE Real and imaginary parts of dielectric constant for ZB of GaAs

(c) BSE Real and imaginary parts of dielectric constant for ZB of GaSb

Figure 4.7: Calculated BSE data for complex dielectric constant for ZB of GaX

The optical properties of a medium are completely described by the real and imaginary parts of a complex dielectric function for various photon energies, as shown in Figure (4.7 a, b, and c). The electron excitation is related to the real part of the dielectric constant's peak value. The zinc-blend(ZB) GaP structure's real part of the dielectric function, illustrated in Figure (4.7(a)), has a maximum peak that emerges approximately 20.68 at a photon energy of 2.94 eV using the GGA-PBE approximation. Similar to this, using the GGA-PBE approximation, the greatest peak of the imaginary component $\varepsilon_1(\omega)$ of the zinc-blende(ZB) GaP structure appears around 23.27 at a photon energy of $3.19eV$. The zinc-blende(ZB) GaAS structure's actual part of the dielectric function, seen in Figure (4.7(b)), has a maximum peak appears around 20.68 at a photon energy of $2.94eV$ using GGA-PBE approximation. Similar to the above, using the GGA-PBE approximation, the imaginary component $\varepsilon_2(\omega)$ of the dielectric function of the zinc-blende(ZB) GaAs structure has a maximum peak that emerges at 165 at a photon energy of $0.96eV$. According to Figure (4.7(c)), the zinc-blende (ZB) GaSb structure's real component $\varepsilon_1(\omega)$of the dielectric function has a maximum peak that emerges around 1.00 at a photon energy of 0.99eV using the GGA-PBE approximation. Similar to this, the zinc-blende (ZB) GaSb structure's imaginary component of the dielectric function, $\varepsilon_2(\omega)$, has a maximum peak that emerges at 9.98 at a photon energy of 1.00eV using the GGA-PBE approximation

The optical properties of a medium are generally explained by the real and imaginary parts of a complex dielectric function for various photon energies, as shown in Figure (4.8(a, b, c)). The electron excitation is connected to the real part of the dielectric constant's peak value. The zinc-blende(ZB) GaP structure's real component of the dielectric function, $\varepsilon_1(\omega)$, is depicted in Figure (4.8(a)). GaP's complex dielectric constant $\varepsilon_1(\omega)$ shows a real portion that grows with photon energy between 0.04 and 3.16 eV. Using the GGA-PBE approximation, its maximum peak value occurs around 17.06 at a photon energy of 3.16 eV. The loss factor increases with an increase in photon energy in this energy range, as seen by the increase in dielectric constant with increase in photon energy in the photon energy ranges of 3.16-3.57eV and 3.57-5.38eV. The real component of the complex dielectric then degrades as photon energy rises, decreasing from a low value of

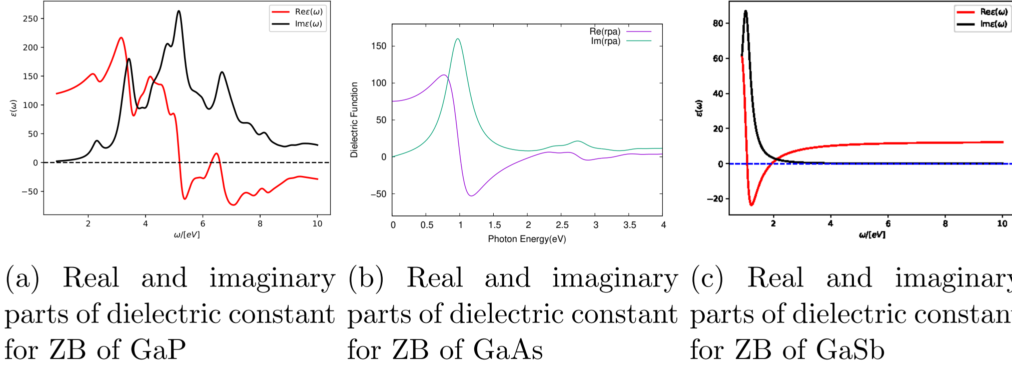

(a) Real and imaginary parts of dielectric constant for ZB of GaP

(b) Real and imaginary parts of dielectric constant for ZB of GaAs

(c) Real and imaginary parts of dielectric constant for ZB of GaSb

Figure 4.8: Calculated RPA data for real and imaginary parts of dielectric constant for ZB of GaX

-5.86 at 7.11eV to a maximum value of 3.57 to 5.38eV. This demonstrates that when photon energy increases in this energy range, the loss factor decreases. Similar to this, the imaginary portion of GaP's complex dielectric constant, $\varepsilon_2(\omega)$, is constant between photon energies of 0.03 and 3.42 eV and 4.01 and 5.16 eV, and it rises as photon energy increases which is in good agreement. Its maximum peak, which is in good agreement, occurs around a value of 20.75 at 5.16 eV. The increase in the complex dielectric's imaginary portion in the photon energy ranges of 2.17-3.75eV and 4.09eV-5.16eV demonstrates that the loss factor rises as photon energy rises in this energy range. In the photon energy range of 0.166.14eV, the imaginary component of the complex dielectric constant falls with an increase in photon energy, with a minimum value of 7.67 at 6.14eV. This demonstrates that when photon energy increases in this energy range, the loss factor decreases. The zinc-blend(ZB) GaAs structure's real component of the dielectric function, $\varepsilon_1(\omega)$, is depicted in Figure (4.8(b)). GaAs's complex dielectric constant $\varepsilon_1(\omega)$ shows a real portion that grows with photon energy between 0.02-0.77eV. Using the GGA-PBE approximation, the maximum peak value is roughly 92.3 at a photon energy of 0.77 eV. The loss factor increases with an increase in photon energy in this energy range, as seen by the increase in dielectric constant with increase in photon energy in the photon energy range of 0.02-0.077eV. In the photon energy range of 0.02-0.77eV, the real component of the complex dielectric then declines with increasing photon energy, reaching a low value of -51.78 at 1.12eV. This demonstrates that when photon energy increases in this energy range, the loss factor decreases. Similar to this, the imaginary portion of GaAs' complex dielectric constant, $\varepsilon_2(\omega)$, is constant in the photon energy range of 0.51-1.35 eV and rises as photon energy rises. Its greatest peak appears approximately 165 at 0.96 eV, which is rather consistent. The loss factor increases with increasing photon energy in this energy range, as demonstrated by the increase in the imaginary portion of the complex dielectric in the photon energy range of 0.51-1.35eV. In the photon energy range of 0.96-1.35eV, with a minimum value of 7.56 at 1.9eV for low photon energies, the imaginary component of the complex dielectric constant falls with an increase in photon energy. Figure (4.8(c)) shown as the real part $\varepsilon_1(\omega)$ of the dielectric function, of zinc-blende(ZB) GaSb structure. The real part of the complex dielectric constant $\varepsilon_1(\omega)$ of GaSb increases with an increase in photon energy in the energy range 0.008-0.78eV. It has a maxmum peak value appears

around 5.22 at a photon energy of 0.78eV using GGA-PBE approximation. The increase in dielectric constant with increase in photon energy in the photon energy range 0.008-0.78eV shows that the loss factor increases with an increase in photon energy in this energy range. The real part of the complex dielectric then decreases with increase in photon energy in the photon energy range 0.78-1.21eV with a minimum value of -1.87 at 1.21eV. This shows that the loss factor decreases with increase in photon energy in this energy range. Similarly the imaginary part of the complex dielectric constant,$\varepsilon_2(\omega)$,of GaSb is constant in the photon energy range 0.012-6.86eV and increases with an increase in photon energy in the energy range 0.012-6.86eV. It has a maximum peakappears around at a value of 6.86 at 1.03eV, which is in good agreement. The increase in the imaginary part of the complex dielectric in the photon energy range 0.59-1.36eV shows that the loss factor increases with increase in photon energy in this energy range. The imaginary part of the complex dielectric constant decreases with an increase in photon energy in the photon energy range 1.03-1.63eV with a minimum value of 0.62 at 1.63eV. This shows that the loss factor decreases with increases in the photon energy in this energy range

. As shown in Figure (4.9(a)) the refractive index spectrum of GaP in the en-

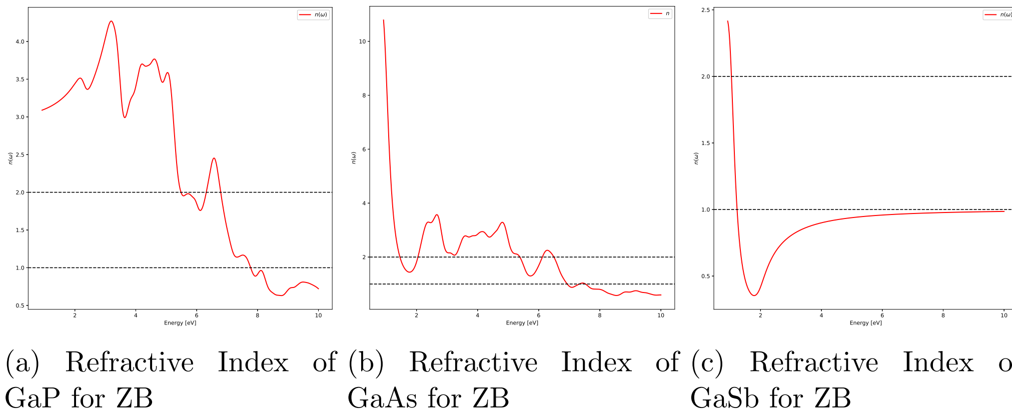

(a) Refractive Index of GaP for ZB (b) Refractive Index of GaAs for ZB (c) Refractive Index of GaSb for ZB

Figure 4.9: Refractive Index for ZB structures of GaX

ergy range 0.85eV to 10.1eV. There is an increase in the refractive index in the energy range 2.0eV to 3.8eV, and 4.0eV to 5.8eV with a peak values of 4.5 value appears around at 3.5eV and 4.8eV. The refractive index decreases afterwards in the energy range 3.5eV to 10.1eV. This decrease in refractive index indicates that GaP shown normal dispersion behaviour. Our result for refactive index is higher than the experimental values(Nelson and Tumer,1968) and (Matsumoto and Kumabe,1979) this difference is suspected to have come from the experimental results taken in this works. Two maximum peaks are observed at 3.5ev and 4.8eV, they are mainly due to transion(Zhang et al). As shown in Figure (4.9(b)) the refractive index spectrum of GaAs in the energy range 0.93eV to 10.1eV. The refractive index of GaAs increases with an increase in photon energy in the energy range 1.72eV to 2.67eV , 3.24eV to 4.81eV, 4.81eV- 5.72eV and 5,72eV to 6.28eV. It has a peak values of 3.29 at 4.81eV,and 2.29 at 6.28eV. The refractive index decreases afterwards in the energy range 4.81eV- 5.72eV and 6.28eV- 9.96eV. This decrease in the refractive index indicates that GaAs shows normal dispersion behaviour. Two peaks are observed at 4.81eV and 6.29eV they are mainly due

to transion. Our result for the refractive index is higher than that reported by Blakemore($3.78eV$)[21] and Brian et al ($3.6eV$)[23]. As shown in Figure (4.9(c)) the refractive index of GaSb increases with an increase in photon energy in the energy range 0.92eV to 1.73eV. It has a maximum values of 0.374 value appears around at 1.73eV. The refractive index decreases afterwards in the energy range 1.73eV to 9.96eV. This decrease in refractive index indicates that GaSb shown normal dispersion behaviour. Our result for refactive index is in good agreement with the reported values (Adachi(1989)(1.73eV) ,Aspnes and Studna(1983) (Brain et al 1.73eV) this difference is suspected to have come from the experimental results taken in this works

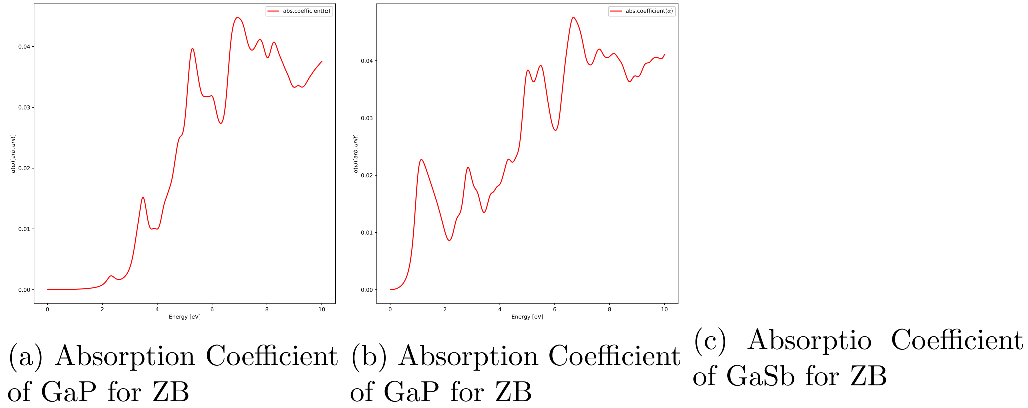

(a) Absorption Coefficient of GaP for ZB (b) Absorption Coefficient of GaP for ZB (c) Absorptio Coefficient of GaSb for ZB

Figure 4.10: Absorption Coefficient for ZB structures of GaX

As shown in figure (4.10(a)) the absorption coefficient α of GaP increases with an increase in photon energy in the energy range 0.007-2.27eV, 2.66eV-3.48eV, 4.02eV-5.27eV, 6.26eV-6.93eV, 7.38eV-7,76eV and 7.99eV-8,26eV. It has a peak values appear around $0.00237(2.37 \times 10^8 m^{-1} = 23.7 \times 10m^{-1})$ $0.0153(1.53 \times 10m^{-1})$, $0.0398(3.98 \times 10m^{-1})$, $0.0449(4.49 \times 10m^{-1})$, $0.04124(4.12 \times 10m^{-1})$ and $0.04067(4.07 \times 10m^{-1})$ at values of 2.29eV, 3.48eV, 5.27eV, 6.93eV, 7.76eV and 8.26eV which is in agreement with that reported by Dean and Thomas($10cm^{-1}$) (Dean and Thomas, 1966), and Dean et al($10cm^{-1}$) (Zhang et al; 2011). (Dean et al, 1967). The value of the absorption coefficient then drops to a value of $0.0376 \times 10m^{8-1}$ at 10eV. This high value of the absorption coefficient is typical for interband absorption in semiconductors. It is important to emphasize that there is no absorption in the energy range 0.02eV-1.81eV which is the energy range of the bandgap of GaP. That is, the energy at which the absorption starts correspond to the direct band gap at 1.81eV. GaP shows no absorption below its band gap, that is, the energy at which the absorption starts corresponds to the direct band gap at 2.41eV (Panish and Casey,1969). GaP shows no absorption below its band gap. The absorption coefficient shows five peaks at photon energies 2.29eV, 3.48eV, 5.27eV, 6.93eV, 7.76eV and 8.26eV, they are mainly due to transition. As shown in figure (4.10(b)) the absorption coefficient α of GaAs increases with an increase in photon energy in the energy range0.02eV-1.17eV, 2.16eV-2,84eV, 3.38eV-5.03eV and 5.99eV-6.67eV. It has a maximum value of $0.0227 \times 10^8 m^{-1}$, $0.089 \times 10m^{8-1}$ $0.0385 \times 10m^{8-1}$, and $0.0478 \times 10m^{8-1}$ at 1.13eV, 2,84eV, 5,05eV,and 6,67eV which is in agreement with that reported by Sturge ($5 \times 10^4 cm^{-1}$[26]), Blakemore

($5 \times 10^4 cm^{-1[21]}$) and Aloulou et al.($10^5 cm^{-1[27]}$). The value of the absorption coefficient then drops to a value of $0.05 \times 10^8 m^{-1}$ at 10.0 eV. This high value of the absorption coefficient is typical for interband absorption in semiconductors [26]. It is important to emphasize that there is no absorption in the energy range 0.026.7eV which is the energy range of the bandgap of GaAs. That is, the energy at which the absorption starts correspond to the direct band gap at 1.52eV ref6 . GaAs shows no absorption below its band gap. The absorption coefficient shows four peaks at photon energies 1.13eV, 2.84eV, 5.03eV and 6.67eV. As shown in Figure4.10(c) the absorption coefficient α of GaSb increases with an increase in photon energy in the energy range 0.007eV-1.17eV. It has a maximum value of $0.00475 \times 10^8 m^{-1}$, at 1.17eV which is in agreement with that reported by Qiao et al.(1990)($1.0 \times 10^5 cm^{-1}$. The value of the absorption coefficient then drops to a value of $3 \times 10^8 m^{-1}$ at 10.0 eV. This high value of the absorption coefficient is typical for interband absorption in semiconductors [26]. It is important to emphasize that there is no absorption in the energy range 3.7510eV which is the energy range of the bandgap of GaSb. That is, the energy at which the absorption starts correspond to the direct band gap at 0.92eV . GaSb shows no absorption below its band gap. The absorption coefficient shows peaks at photon energies 1.17eV

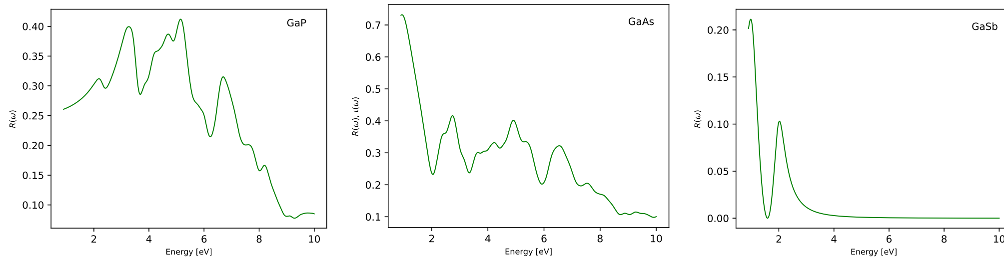

(a) Reflectance of Gallium Phosphide (GaP) for ZB (b) Reflectance of Gallium Arsenide(GaAs) for ZB (c) Reflectance of Gallium Antimonide(GaSb) for ZB

Figure 4.11: Reflectance for ZB structures of GaX

As shown in figure (4.11(a)) the reflectance of GaP increases with the increase in the photon energy in the energy range 3.69-5.11eV. It has a maximum value is 0.412 at 5.11eV, which is in good agreement with that reported by Zhang et al(2011)(4.0eV). Four peaks were observed at 2.19eV, 3.27eV, 5.11eV and 6.71eV. As shown in Figure (4.11(b)) the reflectance of GaAs increases with an increase in photon energy in the energy range 2.032.76eV . It has a maximum value is 0.417 at 2.76eV which is the reflectance obtained by us is in good agreement with that reported by El-Nahass et al. (2.03)[29] and Phillipp and Ehrenreich (0.42 at $2.06eV$)[30]. Three peaks were observed at 2.76eV, 4.90eV, and 6.58eV. As shown in Figure (4.11(c)) the reflectance of GaSb increases with an increase in photon energy in the energy range 1.5ev2.03eV . It has a maximum value is 0.1019 at 2.03eV which is the reflectance obtained by us is in good agreement with that reported ($o.1013$)[29]and ($0.1016eV$)[30]. The peak was observed at 2.03eV. The high value of the reflective of GaSb is highly absorbing and the minimum value Which it drops point value of $3.0 \times 10^8 m^{-1}$ at 10.0eV is no absorbation.

4.2 Structural and Electronic properties of graphene/GaX erostructure

4.2.1 Structural properties of graphene/GaX (X=P, As, Sb)heteroju

We considered the adsorption of graphene on GaX(X=P,As,Sb) heterostructure.The adsorption energy is defined as:

$$E_{ads} = E_{total(graphene-GaX)} - E_{GaX} - E_{GaX} - E_{graphene} \tag{4.4}$$

$$E_{ads} = \frac{(E_{totalgraphene-GaX} - E_{GaX} - E_{graphene})}{n} \tag{4.5}$$

. where E_{ads} is the adsorption energy per C atom (eV);$E_{totalgraphene-GaX}$, $E_{graphene}$ and E_{GaX} is the total energy of the interface,graphene and GaX(X=P,As,Sb) structures,respectively; n is the total number of carbon atoms in the graphene layers. Figure (**??**) shows that the adsorption behaviors of the three configurations for GaP,GaAs and GaSb and $(000\bar{1})$ surfaces are almost the same. More importantly,the long range vdW interaction plays an important role in the adsorption

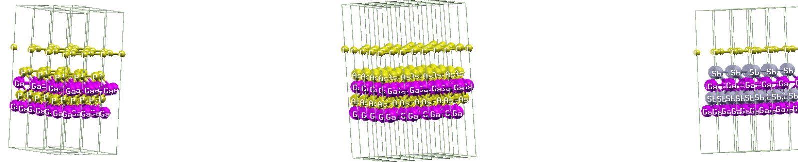

(a) Graphene/GaP heterojunction structure (b) Graphene/GaAs heterojunction structure (c) Graphene/GaSb heterojunction structure

Figure 4.12: Graphene/GaX heterojunction structure

Cohseive and Formation energy of graphene/GaX (X=P, As, Sb) heterostructure

As shown in table (4.4), the computed cohesive energy are $-33.163eV/atom$, $-49.615eV/atom$ and $-72.728eV/atom$ for GaP, GaAs and GaSb respectively. We are implies that GaP > GaAs > GaSb depending up on the calculated values of cohesive energy(E_{coh}). When we compared the three materials GaAs, GaSb and GaP with to each others, the cohesive energy values are described as -33.163eV/atom > -49.615eV/atom > -72.728eV/atom that means the value of GaP is greater this implies that more stable than the remaining of the twos. During calculation GaX(GaP,GaAs and GaSb) are taken as face-center-cubic structure(FCC). The computed formation energies(E_f) values are 75.422eV, 52.543eV, and 34.014eV

Table 4.4: Computed the lattice constant $a(\text{Å})$, the bulk modulus $B(GPa)$, formation energy $E_f(eV/atom)$, and the cohesive energies $E_{coh}(eV/atom)$ of selected graphene/ GaP,GaAs and GaSb materials systems of Heterostructure

Quantity	Materials Source	GaP	GaAs	GaSb
a(Å	This work	5.54	5.76	6.21
	Experimental	5.45eV[a]	5.65[a]	6.10[a]
B(GPa)	This Work	77.3GPa	52.4GPa	46.0GPa
	Experimental	88[b]	75.5GPa[b]	56.3GPa[b]
E_f	This Work	34.014eV	52.543eV	75.422eV
	Experimental	-	-	-
E_{coh}	This Work	-33.164eV	-49.615eV	-72.728eV
	Experimental	6.75eV[c]	-	-

for GaSb, GaAS, and GaP respectively. In terms of formation energy (E_f) described as GaP < GaAS < GaSb that means 34.014eV < 52.543eV < 75.422eV (see table 4.2). From the minimum energies see table. 4.2 which are all negatives. Such a negative values of E_{coh} implies that the GaX(X= P, As, Sb) phases are energetically favorable formed from the point of view of thermodynamics and this stable structure is the most likely to be during this work. Furthermore, the bulk modulus(B) values are 77.3GPa > 52.4GPa > 46.0GPa for GaP > GaAs > GaSb means that GaP has relatively better operating and endurance capacity under pressures. The fact that the optimal geometry structure properties presented in table 4.2 compare reasonably well with experiment values also gives the author a full confidence on the genuineness of the model that is being used in this study.

Cohesive Energies($E_{coh}(eV/atom)$) versus equilibrium distance(d) GaP,GaAs and GaSb materials systems of Heterostructure

Table 4.5: Cohesive Energies ($E_{coh}(eV/atom)$) versus equilibrium distance(d) GaP material systems of Heterojunction

Numbers	1	2	3	4
Cohesive Energies(eV)	35.93	34.42	34.05	33.99
Equilibrium distance(d)	0.52	0.28	0.00	-0.32

Table 4.6: Cohesive Energies ($E_{coh}(eV/atom)$) versus equilibrium distance(d) GaAs material systems of Heterojunction

Numbers	1	2	3	4
Cohesive Energies(eV)	56.80	53.31	52.61	52.50
Equilibrium distance(d)	0.52	0.28	0.00	-0.32

. As shown in table (4.7), the computed cohesive energy are 34.59eV, 53.81eV and 80.52eV for GaP, GaAs and GaSb respectively. We are implies that GaSb > GaAs > GaP depending up on the calculated values of cohesive

Table 4.7: Cohesive Energies ($E_{coh}(eV/atom)$) versus equilibrium distance(d) GaSb material systems of Heterojunction

Numbers	1	2	3	4
Cohesive Energies(eV)	93.87	77.73	75.42	75.06
Equilibrium distance(d)	0.52	0.28	0.00	-0.32

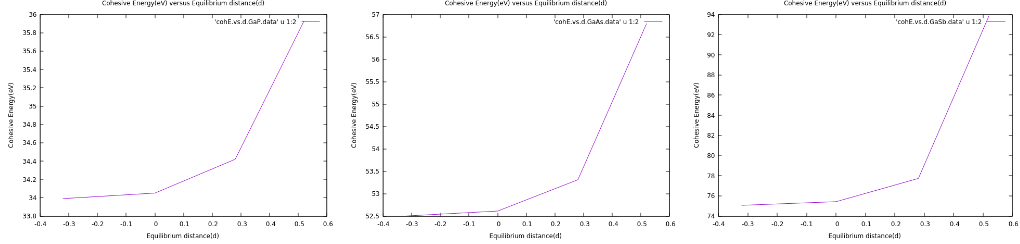

(a) $E_{coh}(eV/atom)$ Vs d GaP material systems of Heterojunction

(b) $E_{coh}(eV/atom)$ Vs d GaAs material systems of Heterojunction

(c) $E_{coh}(eV/atom)$ Vs d GaSb material systems of Heterojunction

Figure 4.13: Cohesive Energies versus equilibrium distance(d) GaP,GaAs and GaSb materials systems of Heterostructure

energy(E_{coh}). When we compared the three materials GaAs, GaSb and GaP with to each others, the cohesive energy values are described as 80.52eV > 53.81eV > 34.59eV that means the value of GaSb is greater this implies that more stable than the GaAs and GaP

Formation Energies($E_f(eV)$) versus equilibrium distance(d) GaP,GaAs and GaSb materials systems of Heterostructure

Table 4.8: $E_f(eV)$ Vs equilibrium distance(d) GaP material systems of Heterojunction

Numbers	1	2	3	4
Formation Energies(eV)	-35.01	-35.57	-33.16	-33.14
Equilibrium distance(d)	0.52	0.28	0.00	-0.32

Table 4.9: $E_f(eV)$ Vs equilibrium distance(d) GaAs material systems of Heterojunction

Numbers	1	2	3	4
Formation Energies(eV)	-53.88	-50.39	-49.68	-49.57
Equilibrium distance(d)	0.52	0.28	0.00	-0.32

As shown in table (4.10) the formation energy (E_f) described as GaP > GaAS > GaSb that means -34.22eV > -50.88eV > -77.82eV (see table (4.10). From the minimum energies see table4.10 which are all negatives. Such a negative values of E_f implies that the GaX(X= P, As, Sb) phases are energetically favorable

Table 4.10: $E_f(eV)$ Vs equilibrium distance(d) GaSb material systems of Heterojunction

Numbers	1	2	3	4
Formation Energies(eV)	-91.16	-75.03	-72.71	-72.36
Equilibrium distance(d)	0.52	0.28	0.00	-0.32

-graph.png -graph.png

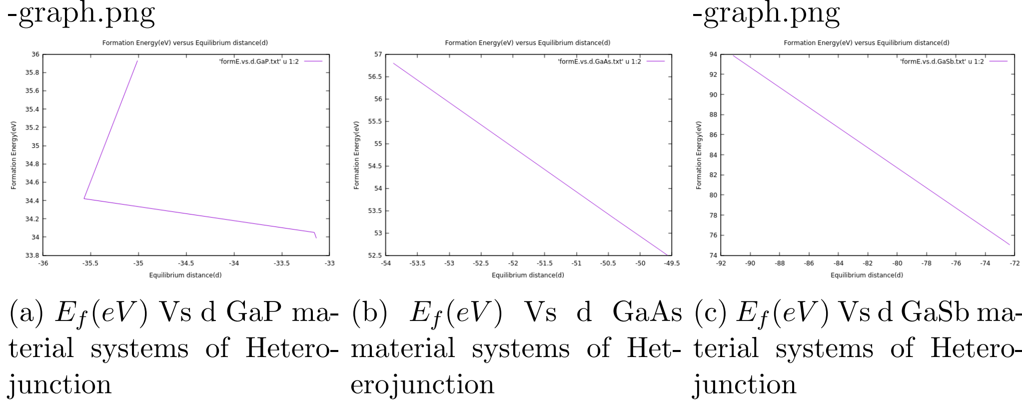

(a) $E_f(eV)$ Vs d GaP material systems of Heterojunction (b) $E_f(eV)$ Vs d GaAs material systems of Heterojunction (c) $E_f(eV)$ Vs d GaSb material systems of Heterojunction

Figure 4.14: Formation Energies versus equilibrium distance(d) GaP,GaAs and GaSb materials systems of Heterostructure

formed from the point of view of thermodynamics and this stable structure is the most likely to be during this work. When we compared the three materials GaAs, GaSb and GaP with to each others, the formation energy values are described as -34.22eV > -50.88eV > -77.82eV that means the value of GaP is greater this implies that more stable than the GaAs and GaSb

Energy per atom versus equilibrium distance(d) GaP,GaAs and GaSb materials systems of Heterostructure

Table 4.11: $Eperatom(eV)$ Vs equilibrium distance(d) GaP material systems of Heterojunction

Numbers	1	2	3	4
Energy per atom	-61.40	-59.51	-59.04	-58.97
Equilibrium distance(d)	0.52	0.28	0.00	-0.32

Table 4.12: *Eperatom* Vs equilibrium distance(d) GaAs material systems of Heterojunction

Numbers	1	2	3	4
Energy per atom	-87.21	-82.84	-81.96	-81.83
Equilibrium distance(d)	0.52	0.28	0.00	-0.32

Table 4.13: *Eperatom* Vs equilibrium distance(d) GaSb material systems of Heterojunction

Numbers	1	2	3	4
Energy Per atom	-133.31	-113.15	-110.25	-109.81
Equilibrium distance(d)	0.52	0.28	0.00	-0.32

per atom -graph.png atom.png Eper atom -graph.png

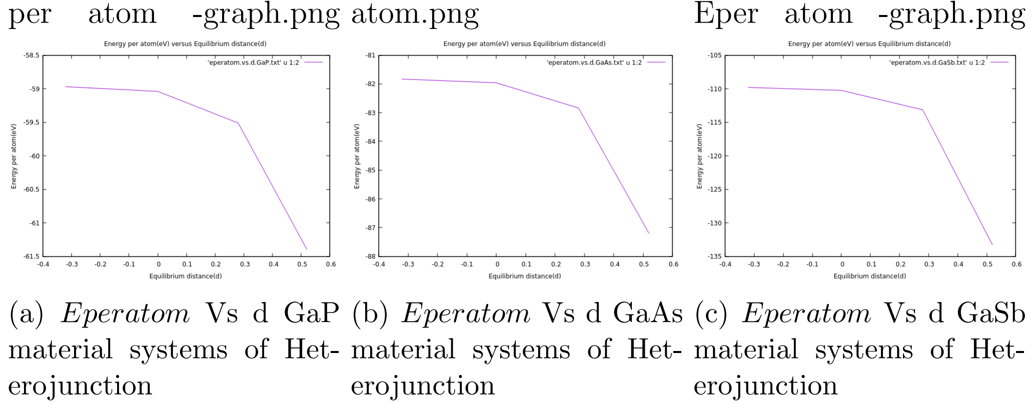

(a) *Eperatom* Vs d GaP material systems of Heterojunction (b) *Eperatom* Vs d GaAs material systems of Heterojunction (c) *Eperatom* Vs d GaSb material systems of Heterojunction

Figure 4.15: Energy per atom versus equilibrium distance(d) GaP,GaAs and GaSb materials systems of Heterostructure

As shown in table 4.13 the energy per atom (*Eperatom*) described as GaP > GaAS > GaSb that means -59.73eV > -83.46eV > -116.63eV (see table4.13). From the minimum energies see table4.13 which are all negatives. Such a negative values of E_f implies that the GaX(X= P, As, Sb) phases are energetically favorable formed from the point of view of thermodynamics and this stable structure is the most likely to be during this work. When we compared the three materials GaAs, GaSb and GaP with to each others, the energy per atom values are described as -59.73eV > -83.46eV > -116.63eV that means the value of GaP is greater this implies that more stable than the GaAs and GaSb

Band gap heterostructure of GaX (X=P, As, Sb)

Table 4.14: Computed the band gap of the calculated and experimental values of GaP, GaAs,and GaSb materials systems of heterostructures

Materials	(a)Å	Sources	Direct	Calculated bandgap(eV)
GaP	5.45	This Work	0.00	
		Experimental	2.41	1.59
GaAs	5.65	This Work	0.00	
		Experimental	1.42	1.019
GaSb	6.10	This Work	0.00	0.60
		Experimental	0.73	0.659

Density of state for graphene/GaX (X=P, As, Sb) Heterostructures

There are three different configurations (GaP, GaAS, and GaSb) that are considered and analyzed in this study. By Using GPAW software, the plain band structure and projected band structures for all heterostructures are plotted and shown as in figure below.

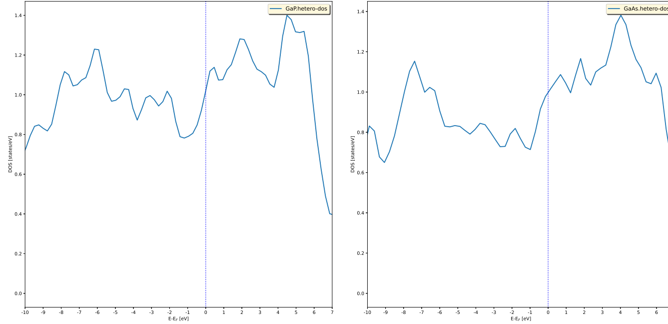

(a) Density of state for heteroStructure of GaP

(b) Density of state for heteroStructure of GaAs

(c) Density of state for heteroStructure of GaSb

Figure 4.16: Density of state heterostructure for GaX (X = P, As and Sb)

As shown in figure4.16,the graphene/GaP heterojunction showed a narrow sharp peak in the DOS at $\sim 4eV$ to $\sim 6eV$ which is associated with a large quantity of generated states in the valence band and nonzero DOS at the Fermi energy indicating that graphene/GaP has a metalic character and as shown in figue4.16,the graphene/GaAs heterojunction showed a narrow sharp peak in the DOS at$\sim 3eV$ to $\sim 6eV$ which is associated with a large quantity of generated states in the valence band and nonzero DOS at the Fermi energy indicating that graphene/GaAs has a metalic character and the same characteristics for the graphene/GaSb

Absroption Energy of GaX (X=P, As, Sb) on graphene

We,studies using the implementation of the DFT based rst principles calculations output, we calculated an adsorption of a compound semiconductor of GaP,GaAS and GaSb are -58.4678,-17.0681 ,and 8.1458 heterojunction on graphene respectively. This results are presented GaSb >GaAs>GaP then 8.1458 >-17.0681>-58.4678

Absorption Energy of graphene/GaX (X=P, As, Sb) heterostructure data

As shown in the table4.15 the computed values of absorption energy per atom are 22.1584eV,34.7554eV,and 48.6314eV. Therefore, graphene with GaP,GaAs,and GaSb are expected to have different electronic properties. Finally, our result shows that the GaSb is higher absorbate coverage than GaAs and GaP. Which means the gallium antimonide compound higher carrier mobilities reactivity and more stability than the compounda of GaAs and GaP. The charge of this compound is transfer

Table 4.15: Absorption Energy of graphene/GaX(X=P, As, Sb) Heterostructure data

Quantity	Materials Source	GaP	GaAs	GaSb
$E_{ads} - GaX - B3$ hetero.dat	This work	-472.0034	-655.0345	-879.9517
	Experimental	-	-	-
$E_{ads} - graphene$ GaX-B3.dat	This Work	-59.0004	-81.8793	-109.9939
	Experimental	-	-	-
$E_{tot} graphene$ layer.dat	This Work	-129.0085	-129.0085	-129.0085
	Experimental	-	-	-
$E_{tot} graphene$ layer per atom.dat	This Work	-16.1261	-16.1261	-16.1261
	Experimental	-	-	-
$E_{tot} - GaX - B3$ clean.data	This Work	-11.5403	-30.0611	-27.1604
	Experimental	-	-	-
$E_{tot} - GaX - B3$ clean per atom.data	This Work	-1.4425	-3.7576	-3.3950
	Experimental	-	-	-

to graphene. Therefore, while considering some experimental calculations, the effect of substrate and should always be considered in order to interpret the data accurately. The most favorable adsorptions have adsorption energies in the range $[-58.47, -17.07, 8.15]eV$ for a carbon adsorbate at $1ML$ adsorbate coverage. With the adsorption of graphene, these values are in the range of $[22.16, 34.76, 48.63]eV$. The relatively lower adsorption energies of carbon compared to graphene could indicate that the respective ions have better mobility within the electrolyte. Furthermore, GaSb is a more favorable as well as reactive surface with the adsorbates at higher fuel supplies, thus, it better represents a typical surface of GaAs alloy. A charge of about $0.261e$ per carbon atom appears to be released to the system for electricity contribution. Finally, the importance of graphenes superior conductivity is not impacted by its interaction with GaX,according to the fact that its Dirac point is unaffected despite its adsorption on GaX. In hybrid systems,excited electrons with energies between 0 and 3eV (against Fermi energy) are primarily accumulated on graphene. The calculations offer a theoretical justification for the successful operation of graphene/GaX hybrid materials as photocatalysts and solar cells

Electron Density(ED), Charge density,and Charge Distribution of the compound GaX (X=P, As, Sb)

The electron density(ED) is used to express by two different ways. The first way is the point specific electronic charge. The electronic density is an electric charge divided by a volume. The system of units adopted is the atomic unit system (a.u) of charge(e) and atomic unit of length (Bohr), which makes the unit equal to the number of electrons per unit of volume. The second way is the density of electronic distribution or the density of probability of presence $\rho(r)$ which is the basis of the density functional theory. Here, The total electronic density is obtained by summing the orbital densities. Let be an atom described by occupied

orbitals Ψ_{nk} each carrying neither electrons($n_i = 1or2$). The total charge density is expressed as follow:

$$\rho(r) = e\sum_{nk}^{occ}|\Psi_{nk}(r)|^2 = en_i(r) \tag{4.6}$$

Atoms with in bulk materials have a net charge. An elegant method that is applicable within plane-wave calculations is the Bader decomposition, which uses stationary points in the three-dimensional electron density to partition electrons among different atoms.From the DFT output data/files ACF(Atomic Chage File/data),BCF(Bader Charge File/data), and AVF(Atom Volume File/data) as shown in table(4.6, 4.7,4.8) of bulk GaP,GaAs and GaSb

ACF/data DFT output of zinc-blende for GaX (X=P, As, Sb)

ACF/data contains the coordinates of each atom, the charge associated with it according to Bader partitioning, percentage of the whole according to Bader partitioning and the minimum distance to the surface. This distance should be compared to maximum cut-off radius for the core region if pseudo potentials have been used
BCF/data contains the coordinates of each Bader maxima, the charge within that volume, the nearest atom and the distance to that atom
AVF/data contains the number of each volume that has been assigned to each atom

ACF/data DFT output of zinc-blende for GaP

Table 4.16: ACF.data DFT output of Zinc-Blende(ZB) fo GaP

Atoms	X	Y	Z	Charge	MIN DIST	ATOMIC VO
Ga	0.000000	0.000000	0.000000	30.020171	1.911083	102.217036
P	2.621995	2.621995	2.621995	15.979250	2.366257	186.192818
Ga	5.243990	5.243990	0.000000	30.020171	1.911056	102.217036
P	7.865985	7.865985	2.621995	15.979250	2.366231	186.192818
Ga	5.243990	0.000000	5.243990	30.020171	1.911056	102.217036
P	7.865985	2.621995	7.865985	15.979250	2.366231	186.192818
Ga	0.000000	5.243990	5.243990	30.020171	1.911056	102.217036
P	2.621995	7.865985	7.865985	15.979250	2.366231	186.192818

VACUUM CHARGE: 0.0000
VACUUM VOLUME: 0.0000
NUMBER OF ELECTRONS: 183.9977

Table4.16revealing that 0.0023 electrons has transferred from phosphide atom to the gallium atom. The atom volume data files in (4.8),are cube files for each Bader volume,describing the density within that volume.(That means it

Table 4.17: BCF DFT output of Zinc-Blende(ZB) fo GaP

Atoms	X	Y	Z	CHARGE	ATOM	DISTANCE
Ga	0.0000	0.0000	0.0000	30.0202	1	0.0000
P	7.8660	7.8660	2.6220	15.9793	4	0.0000
Ga	2.6220	2.6220	2.6220	15.9793	2	0.0000
P	0.0000	5.2440	5.2440	30.0202	7	0.0000
Ga	2.6220	7.8660	7.8660	15.9793	8	0.0000
Ga	5.2440	0.0000	5.2440	30.0202	5	0.0000
P	5.2440	5.2440	0.0000	30.0202	3	0.0000

Table 4.18: AVF/data DFT output of Zinc-Blende(ZB) for GaP

Atoms	Volume(s)
Ga	1
P	3
Ga	8
P	2
Ga	7
P	5
Ga	4
P	6

is just the original cube file,truncated to zero outside the domain of the specific Bader volume). At AVF.dat is a cube file with an integer value at each grid point,describing which Bader volume it belongs to them

ACF/data DFT output of zinc-blende for GaAs

Table 4.19: ACF.data DFT output of zinc-blende for GaAs

Atoms	X	Y	Z	CHARGE	MIN DIST	ATOMIC VO
Ga	0.000000	0.000000	0.000000	30.215191	1.975697	110.702804
As	2.669238	2.669238	2.669238	33.785518	2.408900	193.586552
Ga	5.338476	5.338476	0.000000	30.215191	1.975674	110.702804
As	8.007714	8.007714	2.669238	33.785518	2.408877	193.586552
Ga	5.338476	0.000000	5.338476	30.215191	1.975674	110.702804
As	8.007714	2.669238	8.007714	33.785518	2.408877	193.586552
Ga	0.000000	5.338476	5.338476	30.215191	1.975674	110.702804
As	2.669238	8.007714	8.007714	33.785518	2.408877	193.586552

VACUUM CHARGE: 0.0000.
VACUUM VOLUME: 0.0000.
NUMBER OF ELECTRONS: 256.0028

Table4.19 revealing that 0.0028 electrons has been transferred from arsenide atom to the gallium atom

ACF/data DFT output of zinc-blende for GaSb

Table 4.20: ACF.data DFT output of zinc-blende for GaSb

Atoms	X	Y	Z	CHARGE	MIN DIST	ATOMIC VOL
Ga	0.000000	0.000000	0.000000	30.659011	2.127008	140.736528.
Sb	2.881832	2.881832	2.881832	51.341276	2.634389	242.185470.
Ga	5.763665	5.763665	0.000000	30.659079	2.127000	140.780131.
Sb	8.645497	8.645497	2.881832	51.341231	2.634381	242.156230.
Ga	5.763665	0.000000	5.763665	30.659079	2.127000	140.780131.
Sb	8.645497	2.881832	8.645497	51.341231	2.634381	242.156230.
Ga	0.000000	5.763665	5.763665	30.659093	2.127000	140.788852.
Sb	2.881832	8.645497	8.645497	51.341246	2.634381	242.165977.

VACUUM CHARGE: 0.0000.
VACUUM VOLUME: 0.0000.
NUMBER OF ELECTRONS: 328.0012

Table4.20 indicates that 0.0012 electrons has transferred from antimonide atom to the gallium atom

ACF hetero.data DFT output of Graphene/GaX (X=P, As, Sb) Heterostructures

Table 4.21: ACF hetero.data DFT output of graphene/GaP Heterojunction

Atoms	X	Y	Z	CHARGE	MIN DIST	ATOMIC VOL
C	0.000000	0.000000	22.676714	6.074394	1.264465	102.809446
C	2.333812	1.347427	22.676714	5.952611	1.179338	98.606122
Ga	10.487980	0.000000	9.448631	30.302103	0.915476	107.525771
P	13.109975	2.621995	12.070626	16.929722	0.937017	33.140554
Ga	15.731970	5.243990	9.448631	30.597771	0.957341	113.287172
P	18.353965	7.865985	12.070626	15.095576	0.912517	23.473107
Ga	15.731970	0.000000	14.692621	29.664610	1.029023	19.595342
P	18.353965	2.621995	17.314616	16.475632	0.984790	49.000193
Ga	10.487980	5.243990	14.692621	30.350363	1.010035	22.980494
P	13.109975	7.865985	17.314616	14.555608	0.983823	35.712796

VACUUM CHARGE: 0.0000
VACUUM VOLUME: 0.0000
NUMBER OF ELECTRONS: 195.9984

Table4.21 revealing that 0.027 electrons has been transferred from gallium phosphide atoms to the graphene atoms. This shows that graphene has an excess number of electrons and become an n-type semiconducter and GaP has also losses 0.027 electrons and become a p-type semiconductors

Table 4.22: ACF hetero.data DFT output of graphene/GaAs Heterojunction

Atoms	X	Y	Z	CHARGE	MIN DIST	ATOMIC VOL
C	0.000000	0.000000	22.676714	6.209454	1.264466	108.655690
C	2.333812	1.347427	22.676714	5.856539	1.179338	96.298273
Ga	10.676953	0.000000	9.448631	30.527395	0.910589	105.102168
As	13.346191	2.669238	12.117869	33.713233	0.899403	28.911580
Ga	16.015429	5.338476	9.448631	30.622428	0.926785	108.450489
As	18.684667	8.007714	12.117869	33.885247	0.894744	31.739666
Ga	16.015429	0.000000	14.787107	29.889081	0.960937	18.886347
As	18.684667	2.669238	17.456345	33.571935	0.998248	44.591668
Ga	10.676953	5.338476	14.787107	30.319854	0.981101	20.893630
As	13.346191	8.007714	17.456345	33.402632	0.993552	42.601486

VACUUM CHARGE: 0.0000
VACUUM VOLUME: 0.0000
NUMBER OF ELECTRONS:267.9978

Table 4.12 revealing that 0.066 electrons has been transferred from gallium Arsenide atoms to the graphene atoms. This shows that graphene has an excess number of electrons and become an n-type semiconducter and GaAs has also losses 0.066 electrons and become a p-type semiconductors

Table 4.23: ACF hetero.data DFT output of graphene/GaSb Heterojunction

Atoms	X	Y	Z	CHARGE	MIN DIST	ATOMIC VOL
C	0.000000	0.000000	22.676714	6.043143	1.179340	104.510243
C	2.333812	1.347427	22.676714	6.117604	1.264464	107.755964
Ga	11.527329	0.000000	9.448631	30.644819	0.927077	100.312838
Sb	14.409162	2.881832	12.330463	51.684305	0.919133	33.397713
Ga	17.290994	5.763665	9.448631	30.617857	0.916801	100.397681
Sb	20.172826	8.645497	12.330463	51.839121	0.908140	35.097195
Ga	17.290994	0.000000	15.212295	30.166337	0.982145	19.685446
Sb	20.172826	2.881832	18.094128	51.049604	0.984962	41.116412
Ga	11.527329	5.763665	15.212295	30.208114	0.984540	20.012320
Sb	14.409162	8.645497	18.094128	51.626302	0.983564	43.845185

VACUUM CHARGE: 0.0000
VACUUM VOLUME: 0.0000
NUMBER OF ELECTRONS: 339.9972

Table 4.13 revealing that 0.261 electrons has been transferred from gallium Atimonide atoms to the graphene atoms. This shows that graphene has an excess number of electrons and become an n-type semiconducter and GaSb has also losses 0.261 electrons and become a p-type semiconductors

Electronic charge distribution of bulk GaX (X=P, As, Sb)

The electron density contours denotes the charge distribution in an atom, which in turn also establish the nature of the bond among different atoms. In addition,electronic charge density map serve as a complementary tool for achieving a proper understanding of the electronic structure of the system being studied shown in fig.4.8. The ionic and covalent character of material can be related to charge transfer and sharing between the cation and anion.

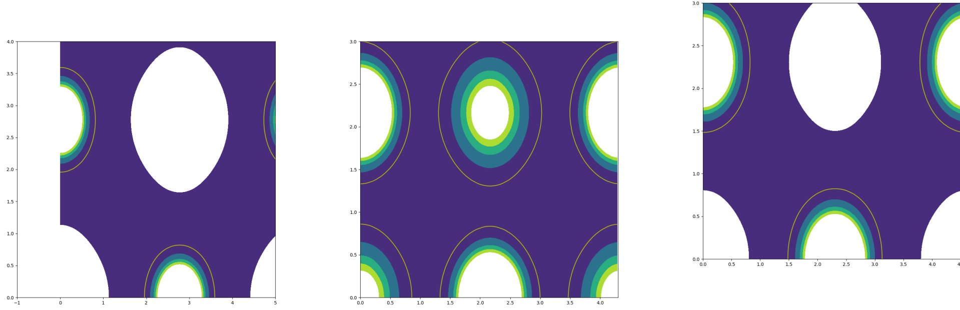

(a) Bader electronic charge density Zinc-Blende(ZB) bulk of GaP

(b) Bader electronic charge density Zinc-Blende(ZB) bulk of GaAs

(c) Bader electronic charge density Zinc-Blende(ZB) bulk of GaSb

Figure 4.17: Bader electronic charge density Zinc-Blende(ZB) of GaX (X = P, As and Sb)

Chapter 5

Conclusion and Recommendations

5.1 Conclusion

In conclusion, we have carried out first principle study of the Electronic structures, electronic, optical properties of the zinc-blende phase for GaX (GaP, GaAs and GaSb) was presented using GPAW package in the frame work of DFT. The exchange-correlation functional is approximated using GGA-PBE, GGA + U. This work was divided into four parts. The first part was devoted to the calculation of the bulk properties, electronic properties, ,optical properties and dynamics properties of GaX(X=P,As,Sb) and graphene. The computed values structure,including equilibrium of lattice parameter, bulk mudulus, cohesive and formation energies of ZB for GaP, GaAs, and GaSb set as 5.54, 5.76, 6.21 as well as B are 77.3GPa, 52.4GPa, and 46,0GPa and 1.43eV, 3.74eV,3.24eV -0.57eV,0,81eV, -0.56eV respectively, which are in a good agreement with the experimental values. The interaction between core and valance electrons was treated using Projector augmented-wave pseudo-potential (PAW) in GGA,PBE and DFT+U approximation for the minimum energy appears

In the second part the electronic properties of ZB GaP, GaAS and GaSb structures including band gap and band structures, DOS and PDOS, electronic charge and charge densities are in a good agreement with the experimental results. In the electronic properties of graphene/GaX(X=P,As,Sb) heterostructure from bader charge,DOS and PDOS were analised.The results shown as there is a charge transfer in between graphene and GaX(X=P,As,Sb) and the combination/junction has no band gap as a conductor

In the thrid part the optical properties including the absorption coefficient,the optical conductivity,the refractive index,the reflection index and the refelectivity

In the fourth part the most favorable adsorptions have adsorption energies in the range [-58.47,-17.07, 8.15]eV for a carbon adsorbate at 1 ML adsorbate coverage. With the adsorption of graphene, these values are in the range of [22.16,34.76, 48.63]eV. The relatively lower adsorption energies of carbon compared to graphene could indicate that the respective ions have better mobility within the electrolyte. Furthermore, the adsorption energies investigated for graphene on GaSb surfaces are desorbable within the PEMFC operating temperature without causing a poisoning effect. GaSb seems to be a preferred structure, compared to GaP,and

GaAs. Furthermore, GaSb is a more favorable as well as reactive surface with the adsorbates at higher fuel supplies, thus, it better represents a typical surface of GaAs alloy. A charge of about 0.261e per carbon atom appears to be released to the system for electricity contribution

5.2 Recommendation and future work

Current studies mainly focused on the First Principles study of novel properties of pristine and carbon supported GaX (X=P, As, Sb)described electronic structures, optical properties of GaX (X=P, As, Sb). Further detailed understanding of lattice parameter,bulk modulus,formation energy, cohesive energy, electronics properties, optical properties, adosrption and heterostructure of GaX doped to graphene material are highly desired. Compact and tunable Mid-IR lasers are of great interest for a variety of applications such as remote chemical sensing, optical communication,solar cell, medical diagnostics and defense require higher output powers than what is currently available. Doping from intrinsically non-magnetic elements with III-V compounds could allow obtaining stable properties at room temperature. For spintronic industry to progress further, stable ferromagnetism in semiconductor materials in form of diluted magnetic semiconductors (DMSs) is electro vital, which can be achieved by incorporation of foreign elemental species in the host materials matrix. Among various gallium X compound semiconductors, GaX (X = P, As and Sb) have garnered intense attention of researchers in both calculated and experimental values owing to their structural stability and optoelectronic properties suited for multifarious applications
Many applications of multinary metal gallium X compound nano-crystals rely on their high collective electrical conductivity. Examples are solar cells, photodetectors and thermoelectric devices. Materials based on ternary and quaternary chalcogenides are known to have large absorption coef-ficients with excellent coverage of the solar spectrum and high stability against solar irradiation and cell. These qualities make them very attractive as light absorbing materials in photovoltaic cells and solar cell
Further research is recommended to determine the pristine structural, electronic, optical, and properties of doped and multinary GaX without substantially changing its crystal structure.

Bibliography

[1] S. M. Sze, Semiconductor Devices, Physics and Technology, (John Wiley & Sons, 1985).

[2] Jivani AR & Jani AR (2012). Prediction of some mechanical and vibrational properties of GaX (X =P, As, Sb) semiconductor compounds. Turkish Journal of Physics, 36 215-223.

[3] Al-Douri Y & Reshak AH (2011). Calculated optical properties of GaX (X=P, As, Sb) under hydrostatic pressure. Applied Physics A, 104 1159-1167.

[4] Reshak AH (2005). First-principle calculations of the linear and nonlinear optical response for GaX (X = P,As, Sb). The European Physical Journal B, 47 503-508.

[5] Froyen S & Cohen MR (1983). Structural properties of III-V zinc-blende semiconductors under pressure. Physical Review B, 28 3258-3265.

[6] Perdew JP, Burke K & Ernzerhof M (1996). Generalized Gradient Approximation Made Simple. Physical Review Letters, 77 3865-3868.

[7] Blaha P, Schwarz K, Madsen GKH, Kvasnicka D Luitz J (2001). WIEN2k, An Augmented Plane Wave Plus Local Orbitals Program for Calculating Crystal Properties, Vienna University of Technology, Austria.

[8] Kittel C (1994). Introduction to Solid State Physics. fifth edition Wiley Eastern, India 210.

[9] L. E. Brus, Electron-Electron and Electron-Hole Interactions in Small Semiconductor Crystallites: The Size Dependence of the Lowest Excited Electronic State, Journal of Chemical Physics, Vol. 80, No. 9, 1984, pp. 4403-4409. doi:10.1063/1.447218.

[10] C.F. Klingshirn, Kling Schoen. Semiconductor Optics [M]. Science Press, (2007)

[11] Arbouche O, Belgoumne B, Soudini B, et al. First-principles study on structural properties and phase stability of III-phosphide (BP, GaP, AlP and InP)[J]. Computational Materials Science, 2010,47(3): 685-692.

[12] Wang Yu, Li Tongwei. Theoretical Study on Lattice Vibration Spectrum of Novel Functional Materials[M]. Beijing: Publishing House of Electronics Industry, 2017.9

[13] Li Yunzhi. Principles of Terahertz Science and Technology[M]. National Defense Industry Press, 2012.

[14] V. R. Ravindran, P.Fjellvg, H. S. BG. Monakhov, E. Ganchenkova, M.Nieminen, Risto M, Phys. Rev.B, 83, 4 (2011)

[15] Hatami F., Masselink W. T., Lordi V.,Harris J. S. 2006. Green emission from InP-GaP squantum-dot light emitting diode, IEEE Photonics Technology Letters 18(7), 895

[16] Epstein A. S., Grove W. O. 1965. Single crystal Gallium Phosphide Solar Cells, Advance Energy Conversion 5(2), 161.

[17] Kish F. A., Steranka F. M., Defevere D.C., Vanderwater D. A., Park K. G., Kuo C.P., Osentowski T. D., Peanasky M. J., Yu J. G., Fletcher R. M., Steigerwald D. A.,Grafford M. G., Robbins V. M. 1994. Very high-efficiency semiconductor wafer-bonded transparent-substrate (Al_xGa_{1-x}) 0.5 In 0.5 P/GaP, lightemitting diodes, Appl. Phys. Lett. 64,2839.

[18] P. Hohenberg, W. Kohn, Inhomogeneous electron gas, Physical review 136 (3B) (1964) B864. URL https://doi.org/10.1103/PhysRev.136.B864

[19] W. Kohn, L. J. Sham, Self-consistent equations including exchange and correlation effects, Physical review 140 (4A) (1965) A1133. URL https://doi.org/10.1103/PhysRev.140.A1133

[20] W. Schiehlen, et al., Multibody systems handbook, Vol. 6, Springer, 1990.

[21] L. Tian, Density Functional Theory study of bulk properties of metallic alloys and compounds, Ph.D. thesis, KTH Royal Institute of Technology (2017).

[22] Capelle K. (2006). A Birds-Eye View of Density-Functional Theory.:-Cond-mat.mtrl-Sci. 1 -69.

[23] M. Size, Physics of Semiconductor Device (John Wiley, and Sons, New York, 1985).

[24] W. Kohn, L. J. Sham, Self-consistent equations including exchange and correlation effects, Phys. Rev. 140 (4A) (1965) A1133A1138. doi:10.1103/PhysRev.140.A1133.

[25] E. Runge, E. K. U. Gross, Density-functional theory for time-dependent systems, Phys. Rev. Lett. 52 (1984) 997 1000.

[26] P. E. Blchl, C. J. Forst, J. Schimpl, The projector augmented wave method: ab-initio molecular dynamics with full wave functions, Bull. Mat. Sci. 26 (2003) 33.

[27] Von. (2007). Structural, Electronics and Optical properties of Gallium Phosphide. Doktorgrades des Naturwissenschaften.1 - 135.

[28] Helmut, E. (1996). The Fundamentals of Density Functional Theory (Springer Vieweg, 1st edn, 1). Solid State and Materials Research. 1 -224.

[29] Dixit, H. (2012). First-principles electronic structure calculations of transparent conducting oxide materials.1 - 179.

[30] Vorgelegt, V. (2009). Density-Functional Theory and Quantum Chemistry Studies on dry and wetNaCl(001). DOCTOR RERUM NATURALIUM. 22.

[31] Hedin, L. and Lundqvist, B. I., (1971). Explicit local exchange correlation-potentials, Journal of Physics C: Solid State Physics 4, 2064-2083.

[32] Heyd, J., Scuseria, G. E. (2004). Efficient hybrid density functional calculations in solids: Assessment of the Heyd-Scuseria-Ernzerhof screened Coulomb hybrid functional. The Journal of chemical physics, 121(3), 1187-1192.

[33] Campo J V. L.,Jr. Cococcioni M., (2009). Extended DFT+U+V method with on-site and intersite electronic interactions. PACS numbers:71.10.Fd, 71.15.Mb, 71.20.

[34] F. Bloch, Quantum mechanics of electrons in crystal lattices, Z. Phys 52 (1928) 555600. URL https://doi.org/10.1098/rspa.1931.0019.

[35] S. groe Holthaus, PhD Dissertation, Molecular Dynamics Simulation of ZnO (AIP, University of Bremen, German, 2014).

[36] G. Lori, E. Law, M. Tan, D.H Montano, M. Goldberger, J. Somorjai, G. Yang, Peidong Nano letters, 5, 7 (2005).

[37] A. N. Morawietz, T.Behler, Jrg. Phys. Rev.B 83, 15 (2011).

[38] M. Fang, M. Dijkstra and A. Van, Physical chemistry (Utrecht University, Netherlands, 2017).

[39] A. Baranv, P. Sokolov, O. Kurakeych, and V. Tafeenko, Material Science Department (Moscow State University, Russia, 2016).

[40] R. M. Martin, Electronic structure: basic theory and practical methods, Cambridge university press, 2020.

[41] O. Jepson, O. Anderson, The electronic structure of hcp Ytterbium, Solid State Communications 9 (20) (1971) 17631767. URL https://doi.org/10.1016/0038-1098(71)90313-9

[42] P. E. Blchl, O. Jepsen, O. K. Andersen, Improved tetrahedron method for Brillouin-zone integrations, Physical Review B 49 (23) (1994) 16223. URL https://doi.org/10.1103/PhysRevB.49.16223

[43] M. Methfessel, A. Paxton, High-precision sampling for Brillouin-zone integration in metals, Physical Review B 40 (6) (1989) 3616. URL https://doi.org/10.1103/PhysRevB.40.3616.

[44] Jumes D., P., and Bernared C., B. (2005). Solid-State Physics (Introduction to the Theory). Berlin Heidelberg New York.

[45] Klingshirn C. (2005). Semiconductor Optics. Springer, Berlin Heidel-berg. vol. 34, 2 nd edn, New York. pp. 1-801.

[46] Liu Li, Wei Jianjun, Turdy Wu Buyer, Feng Yan, Peng Min. First-principles study of the electronic structure, optical properties and anisotropy of GaP[J]. Journal of Atomic and Molecular Physics, 2015, 32(02):336-344.

[47] Zhou H D, Vogt B W, Janik J A, et al. Partial field-induced magnetic order in the spin-liquid kagom Nd3Ga5SiO14[J]. Physical Review Letters, 2007, 99(23):236401.

[48] Raghuveer, C. (2010). Optical Properties of Materials calculated from First Principle Theory.1 - 49.

[49] M. Hybertsen, S. Louie, Ab initio static dielectric matrices from the density-functional approach: Formulation and application to semiconductors and insulators, Phys. Rev. B 35 (1987) 5585, URL https://doi.org/10.1103/PhysRevB. 35.5585.

[50] A. Glass, D. v. Linde, T. Negran, High voltage bulk photovoltaic effect and the photorefractive process in LiNbO3 , Appl. Phys. Lett. 25 (1974) 233, URL https://doi.org/10.1063/1.1655453.

[51] http: //w.w.w physicist forums. com (Last updated: July 2014).

[52] Stolyarova, E. et al. High-resolution scanning tunneling microscopy imaging of mesoscopic graphene sheets on an insulating surface. Proc. Natl. Acad. Sci. U.S.A. 104, 9209-9212 (2007).

[53] Meyer, J. et al. The structure of suspended graphene sheets. Nature 446 ,60-63 (2007).

[54] Carlsson, J. Buckle or break. Nat Mater 6, 801-802 (2007).

[55] Geim, A. Kim, P. Carbon wonderland. Sci. Am. 298 , 90-97 (2008).

[56] Geim, A. Novoselov, K. The rise of graphene. Nat Mater 6 , 183-191 (2007)

[57] Wilson, M. Electrons in atomically thin carbon sheets behave like massless particles. Phys today 59 , 21-23 (2006).

[58] Novoselov, K.S. et al.Two-dimensional gas of massless Dirac fermions in graphene. Nature 438 , 197-200 (2005).

[59] Kbler, J. K. (2000) Theory of Itinerant Electron Magnetism; Seo, D. K. (2006) Density functional perturbational orbital theory of spin polarization in electronic systems.Formalism I. J.

[60] J. Enkovaara, C. Rostgaard, J. J. Mortensen, J. Chen, M. Duak, L. Ferrighi, J. Gavnholt, C. Glinsvad, V. Haikola, H. Hansen, et al., Electronic structure calcu- lations with GPAW: a real-space implementation of the projector augmented-wave method, Journal of Physics: Condensed matter 22 (2010) 253202.

[61] P. E. Blchl, O. Jepsen, O. K. Andersen, Improved tetrahedron method for Brillouin-zone integrations, Physical Review B 49 (1994) 16223.

[62] J. P. Perdew, K. Burke, M. Ernzerhof, Generalized gradient approximation made simple, Physical Review Letters 77 (1996) 3865.

[63] Monkhorst H. J. & Pack J. D. (1976). Special points for Brillouin-zone integrations. Physical Review B. vol. 13, no. 12, pp. 5188 - 5192.

[64] G. Makov, M. Payne, Periodic boundary conditions in ab initio calculations, Phys- ical Review B 51 (1995) 4014.

[65] B. Himmetoglu, A. Floris, S. De Gironcoli, M. Cococcioni, Hubbard-corrected DFT energy functionals: The LDA+ U description of correlated systems, International Journal of Quantum Chemistry 114 (2014) 1449.

[66] S. Grimme, Semiempirical GGA-type density functional constructed with a long- range dispersion correction, Journal of Computational Chemistry 27 (2006) 17871799.

[67] T. Jayasekera, S. Xu, K. W. Kim, M. B. Nardelli, Electronic properties of the graphene/6H-SiC (000 1) interface: A first-principles study, Physical Review B 84 (2011) 035442.

[68] M. Vanin, J. J. Mortensen, A. Kelkkanen, J. M. Garcia-Lastra, K. S. Thygesen, K. W. Jacobsen, Graphene on metals: A van der Waals density functional study, Physical Review B 81 (2010) 081408.

[69] M. Dion, H. Rydberg, E. Schrder, D. C. Langreth, B. I. Lundqvist, Van der waals density functional for general geometries, Physical Review Letters 92 (2004) 246401.

[70] F. Murnaghan, The compressibility of media under extreme pressures, Proc. Natl. Acad. Sci. 30 (1944) 244.

[71] F. Birch, Finite strain isotherm and velocities for single-crystal and polycrystalline NaCl at high pressures and 300 K, J. Geophys. Res. 83 (B3) (1978) 1257.

[72] F. Aryasetiawan and O. Gunnarsso, Phys. Rev.B 54, 8 (1996)

[73] J. Paier, M. Marsman, K.Hummer, G. Kresse, I.J. Angyan, J. Chem. Phys. 124, 154709 (2006)

[74] http://www.Phys.Isu.edu/Ramesh Paudya /Solid materials Phys.Review(2002).

[75] L.Yu.et al., First Prnciples study on Electronic Structure and Optical properties of Ternary GaAs:Bi Alloy.Materials, vol5, 2486-2497(2012).

[76] Dubey.S.K; Dubay, R.L; Yadav,A.D.,V; Rao,T.K.Gundu; Mohanty, T.;Kanjilal,D.(2006).

[77] S.B.Zhang, M.L.Cohen, Phys.Rev.B 35, 7604(1987).

[78] Juan,Y.,and Kaxiras, E.,(1993). Application of gradient correction to DFT for atoms and solids. Phys.Rev.B Vol,48,pp.14944-14952.

Declaration

I declare that the thesis hereby submitted to Addis Ababa University for the degree of Master of Science has not previously been submitted by me for a degree at this or any other university, that it is my own work both in design and execution, and that all material contained herein has been duly acknowledged.

Name: Demmilash Kassa

Signed: – – ––

Date: – – ––

e-mail: welebumakassa1977@gmail.com

Place and time of submission

Addis Ababa University

Department of Physcs

November 10, 2023

This thesis has been submitted for examination with my approval as University adviser.

Name: Dr. Kenate Nemera

Signature: – – ––